INTRODUCTION

HCM (hypertrophic cardiomyopathy) and DCM (dilated cardiomyopathy) are very common types of cardiomyopathy. HCM is characterized by abnormal cardiac hypertrophy, fibrosis and myofibrillar disarray. DCM is defined by ventricular chamber dilation and impaired contractile function. Genetic studies have indicated that approx. half of HCM is familial and caused by a mutation in sarcomeric proteins [1]. Among the causative genes, βMHC (β-myosin heavy chain) is most commonly associated with HCM [2]. Disease penetrance, severe hypertrophy and high risk of sudden cardiac death are more frequently associated with mutations in βMHC than in the other sarcomere protein genes, such as cardiac troponin T, α-tropomyosin and cardiac myosin-binding protein C genes [3]. On the other hand, approx. 25–30% of idiopathic DCM is caused by a missense mutation or deletion in cardiac genes such as βMHC, cardiac troponin T, cardiac actin, lamin A/C and dystrophin [2,4]. In DCM, βMHC mutations are also relevant to early onset and serious cardiac dysfunction [5,6]. In addition, cases in which HCM has progressed to DCM have been reported [7,8]. This progression occurs in 10–15% of patients with HCM [9]. However, the mechanisms whereby mutations of the βMHC gene lead to cardiac hypertrophy or dilation remain unclear. Moreover, it is still not clear whether there is a common aetiology for these diseases.

Transgenic mouse models expressing mutant proteins provide a means of gaining insight into the pathophysiological and clinical features of human cardiomyopathy. For example, transgenic mice carrying the missense mutation p.Arg403Gln in the αMHC gene, the murine analogue of the human βMHC gene, recapitulate the characteristics of human HCM [5,10], whereas homozygous mice for the same transgene develop DCM-like disease [11]. The homozygous mutant transgenic mice of another sarcomeric protein, myosin-binding protein C, are also affected with DCM [12]. However, the mechanisms of the primary cardiac dilation caused by the βMHC mutation are still unclear. This is because animal models bearing the analogous mutation within the sarcomeric protein genes identified in human DCM have not so far been investigated.

In the present study we explored mutations in the sarcomere proteins in a patient with isolated LVNC [LV (left ventricular) non-compaction] and found a novel mutation, p.Met531Arg, in the βMHC. We then generated the αMHC transgenic mice with a p.Met532Arg mutation corresponding with the p.Met531Arg in human βMHC. Although these transgenic mice did not develop LVNC, they showed the pathological changes from HCM to DCM. The results of our present study suggest that HCM and DCM may be closely related pathological conditions rather than independent diseases.

MATERIALS AND METHODS

Patients

The study subjects comprised 99 unrelated patients with DCM (27 familial and 72 sporadic or unknown) and five patients with isolated LVNC (one familial and four sporadic or unknown). The diagnosis of DCM was based on the criteria of the Collaborative Research Group of the European Human and Capital Mobility Project on Familial Dilated Cardiomyopathy [13], i.e. echocardiographic demonstration of depressed systolic function of the left ventricle [LVEF (LV ejection fraction) < 0.45 and/or fractional shortening < 0.25) and a dilated left ventricle [LVEDD (LV end-diastolic diameter) $> 117\%$ of the predicted value corrected for age and body surface area) in the absence of other cardiac or systemic causes. The diagnosis of isolated LVNC was based on the following echocardiographic criteria [14] in four patients: (i) the absence of coexisting cardiac abnormalities; (ii) the presence of a two-layer structure in the myocardium, with a compacted thin epicardial band and a much thicker noncompacted endocardial layer of trabecular meshwork with deep endomyocardial spaces showing a maximal end systolic ratio of noncompacted to compacted layers of > 2; (iii) the predominant localization of the non-compaction in the mid-lateral, apical and mid-inferior walls; and (iv) colour Doppler evidence of deep perfused intertrabecular recesses. One patient (with the βMHC mutation) was diagnosed by postmortem examination because echocardiographic evidence of LVNC was lacking at that time.

Informed consent was obtained from all subjects in accordance with the guidelines of the Bioethical Committee on Medical Research, School of Medicine, Kanazawa University. gDNA (genomic DNA) was purified from white blood cells [15].

Detection of mutation

Oligonucleotide primers used for the amplification of the βMHC gene exons were based on published sequences [16] and sequences obtained from GenBank®. PCR was used for amplification of gDNA, and SSCP (single-strand conformational polymorphism) analysis of this amplified DNA was then performed with a slight modification of a method published previously [17,18]. DNA fragments with abnormal SSCP patterns were sequenced by the dye terminator cycle sequencing method using an automated fluorescent sequencer (ABI Prism™ 310 genetic analyser; PE Biosystems). To increase the probability of detecting the presence of any sequence change, SSCP was carried out at two different temperatures for each exon, and the size of fragments for SSCP was kept at less than 300 bp. Sequence analysis results were validated by restriction enzyme digestion with Eco81I. To confirm the paternity of the subjects, five short tandem-repeat systems TH01, vWA, LPL, F13B and FES/FPS were investigated as

previously described [19]. From the allele distributions of each short tandem-repeat locus, the probability of paternity was calculated based on the allelic frequencies in the Japanese population [20]. Screening for mutations in other genes, including dystrophin, myosin-binding protein-C, α-tropomyosin, cardiac troponin C, cardiac troponin T, cardiac troponin I, cardiac α-actin, lamin A/C, G4.5, ZASP and α-dystrobrevin was performed by direct sequencing in the proband.

Transgenic constructs

Murine αMHC (the analogous gene of the human βMHC) cDNA (5.9 kbp) and the transgenic construct, αMHC clone 918 (9.1 kbp), were generously provided by Dr J. Robbins (University of Cincinnati, Cincinnati, OH, U.S.A.). The αMHC cDNA was mutated using site-directed mutagenesis according to the manufacturer's protocol (Stratagene), which resulted in a p.Met532Arg mutation in the protein. The mutagenic primers used were 5′-CCCATGGGCATCAGGTCCATCCTGGA-GG-3′ and 5′-CCTCCAGGATGGACCTGATGCCC-ATGGG-3′. The mutated cDNA was sequenced to confirm the presence of the correct mutation and the absence of undesired errors during mutagenesis. The mutated αMHC cDNA was subcloned into the SalI site of αMHC clone 918 between the murine αMHC promoter and the human growth hormone polyadenylation site. The transgenic construct was purified by caesium chloride ultracentrifugation and digested with EcoRI to release a 12.1 kbp fragment that was used for microinjection. This fragment was purified by agarose gel electrophoresis, dissolved in 10 mmol/l Tris/HCl (pH 7.5) containing 0.2 mmol/l EDTA and injected into the pronucleus of fertilized zygotes from BDF1 mice. The microinjections were performed at Japan SLC Inc.

Generation of transgenic mice

Founder transgenic mice were identified by hybridization of tail DNA to a ^{32}P-labelled DNA probe corresponding to the human growth hormone 3′-untranslated region (a 630 bp HindIII/EcoRI fragment from the transgenic construct). PCR was also used to identify the transgenic mice. A forward (5′-TGCCCACCAGCCTTGTCCT-AATAA-3′) and a reverse (5′-CAGGGAAGGGA-GCAGTGGTTCAC-3′) primer were derived from the human growth hormone sequence; PCR with these primers produced a 411 bp fragment using DNA of mice harbouring the transgene. Stable transgenic lines were generated by mating founder transgenic mice with non-transgenic BDF1 mice. Male transgenic mice and non-transgenic male littermates were used for analysis. Experiments were conducted according to guidelines for the care and use of laboratory animals in Kanazawa University and safety guidelines for gene manipulation experiments.

RT (reverse transcription)–PCR

RT–PCR was performed to assess the amount of αMHC, βMHC and GAPDH (glyceraldehyde-3-phosphate dehydrogenase) mRNA in wild-type and transgenic hearts. Total RNA was isolated from the heart using the AGTC (acid guanidinium thiocyanate/phenol/chloroform) method [21] and the first strand cDNA was synthesized using standard cDNA synthesis reagents (first strand cDNA synthesis kit for RT–PCR; Roche) according to the manufacturer's protocol. To assess the αMHC transgene expression, PCR cycling was performed at 94 °C for 60 s, 59 °C for 60 s and 72 °C for 60 s for 30 cycles using rTaq (Takara). The forward (5′-GCCGCGCCAGTACTTCATAGGT-3′) and the reverse (5′-TTGCGAGGCTTCTGGAAGTTGTTA-3′) primers were derived from the murine αMHC cDNA sequence. When the PCR product (351 bp) was digested with XhoI, fragments of 248 bp and 103 bp were generated from the endogenous allele, while the 351 bp fragment from the transgene was not digested because the XhoI site was abolished by site-directed mutagenesis. To determine transcript levels of αMHC and βMHC genes, cDNA products were amplified by cycling at 94 °C for 30 s, 55 °C for 30 s and 72 °C for 30 s for 25 cycles using rTaq (Takara). Sequences of primers were as follows: αMHC, 5′-ATCGCCGAGTCCCAGGT-CAAC-3′ and 5′-TATTGGCCACAGCGAGGGTC-TG-3′; βMHC, 5′-GTGCCAAGGGCCTGAATGA-GG-3′ and 5′-AGGGCTGTTGCAAAGGCTCCAG-3′; GAPDH, 5′-ACCACAGTCCATGCCATCAC-3′ and 5′-TCCACCACCCTGTTGCTGTA-3′.

Echocardiography

Echocardiographic studies were performed using a 12-MHz phased array probe and a Sonos 5500 ultrasonograph (Philips Medical Systems). Mice were anaesthetized lightly by intraperitoneal injection of 10 μg/ml of pentobarbital sodium at a dose of 10 μl/g of body mass. Body fur of the upper sternal and subxiphoid areas was shaved and the exposed skin was moistened for better acoustic coupling. M-mode echocardiographs of the left ventricle were recorded at the middle of the left ventricle. IVST (interventricular septal thickness), PWT (posterior wall thickness), LVESD (LV end-systolic diameter) and LVEDD were measured and the percentage FS (fractional shortening) was calculated as (LVEDD−LVESD)/LVEDD.

Histological examination

Mice were anaesthetized, and the hearts were removed while still beating, rinsed in PBS, and fixed in 10% formalin before sectioning. The hearts were dehydrated through a graded alcohol series and embedded in paraffin. Longitudinal 8 μm sections were cut and stained with H and E (Haematoxylin and Eosin or with Azan and examined under an Olympus IX71

microscope. Photomicrographs were obtained with an Olympus DP70 digital camera. For electron microscopic analysis, the hearts were removed while still beating, and immersed in a cardioplegic solution (25 mmol/l KCl and 5 % dextrose in PBS) to ensure complete myocardial relaxation. Blocks of 1 mm^2 were dissected from the left ventricular free wall. The blocks were trimmed, fixed in 2.5 % glutaraldehyde in cacodylate buffer at pH 7.4, postfixed in 2.0 % osmium tetroxide, dehydrated in ethanol in propylene oxide, and embedded in EPOK812 (Oken). Sections were cut at 60 nm, stained with lead citrate and uranyl acetate, and examined with a JEM-1210 transmission electron microscope (JEOL).

Statistical analysis

Statistically significant differences between groups of non-transgenic and transgenic mice were assessed using an unpaired Student's t test. Results are expressed as means $\pm$ S.D. A P value of <0.05 was considered statistically significant.

RESULTS

Baseline characteristics of the study patients

The 99 adult patients with DCM comprised 68 men and 31 women (mean age 58.1 $\pm$ 13.1 years, range 21–82). The three adult patients (aged 29, 57 and 60 years), and two young patients (aged 10 and 13 years) with isolated LVNC comprised two men and three women. In the patient groups with DCM and isolated LVNC, the LVEDD was 64.8 $\pm$ 7.4 mm and 62.4 $\pm$ 12.8 mm respectively, the LVESD was 55.8 $\pm$ 8.2 mm and 54.2 $\pm$ 10.3 mm respectively and the LVEF was 29.1 $\pm$ 9.8 mm and 26.2 $\pm$ 13.7 mm respectively.

A point mutation was found in the βMHC gene of an isolated LVNC patient

SSCP analysis identified polymorphisms in the βMHC gene in 17 patients with DCM (14 with c.189C>T, two with c.732T>C, four with c.1062C>T, one with c.1128C>T and three with c.3027T>C) which have been reported previously [22]. A mutation was found in the βMHC gene derived from the proband, a 14-year-old girl (Figure 1A, II-4) with isolated LVNC. Sequence analysis of the abnormal polymorphism conformer revealed a nucleotide substitution in codon 531, resulting in substitution of a methionine residue by arginine (Figure 1B). This mutation was not detected in 200 control individuals. No other mutations in the βMHC or other genes, including myosin-binding protein-C, α-tropomyosin, cardiac troponin T, cardiac troponin I, actin, lamin A/C, G4.5, ZASP or α-dystrobrevin were identified in this proband.

Cardiac examination of the proband (II-4) revealed left ventricular dilation and diminished contractile function like DCM (Table 1), although she was asymptomatic. Heart failure progressed and she died at the age of 14 in 1999. Figures 1(C) and 1(D) show the ECG and the photograph of the heart at autopsy. The ECG showed left ventricular hypertrophy. In the autopsy, the left ventricle was markedly dilated and prominent numerous trabeculations with intertrabecular recesses were found at the lateral wall, the inferior wall and the apex of the left ventricle. The thickness ratio between the noncompacted and compacted layer was 3–5. Other congenital cardiac malformations were not found. These findings were consistent with isolated LVNC. On microscopic examination, mild vacuolation was evident in the myocytes, and moderate subendocardial fibrosis was observed (results not shown). The endocardium was thickened by fibrous tissue, but no fibroelastosis was identified. Myocyte hypertrophy was not found. She had an identical twin sister (II-3), who had been diagnosed with DCM and also died of heart failure at the age of 13 (Figure 1A).

Table 1 Echocardiographic data in the proband and her identical twin sister

Parameter	II-3	II-4
Sex	Female	Female
Age (years)	13	13
LVEDD (mm)	70	70
LVEDS (mm)	62	58
FS (%)	11	17
IVST (mm)	10	6
PWT (mm)	10	9

We could not find any abnormalities in the parents (Figure 1A, I-1 and I-2), elder sister (II-1) and elder brother (II-2) by clinical examination, and none of them had the p.Met531Arg mutation in the βMHC gene. The presence of this sequence variant was confirmed with restriction enzyme digest analysis. The 201 bp fragment was digested with Eco81I. The T to G transition at nucleotide position 1674 allows cleavage (yielding 16 bp and 185 bp fragments), whereas the wild-type allele is not cut. Only the proband was heterozygous for the T to G base change (Figure 1A). The allele distribution of five short tandem-repeat loci was then examined in the subject's parents to determine the paternity of the proband. The probability of paternity was 0.9873, which was considered to be highly likely. Thus we concluded that the identified p.Met531Arg mutation in the βMHC gene in the proband was *de novo*.

Generation of p.Met532Arg αMHC transgenic mice

To elucidate the importance of p.Met531Arg of βMHC observed in the human patient, we constructed a

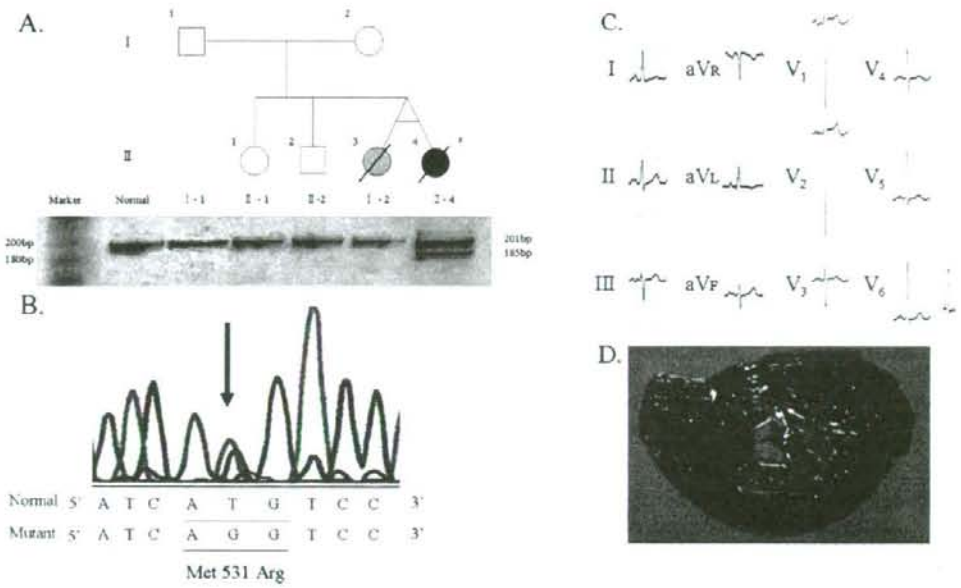

Figure 1 A point mutation was found in the βMHC gene of an isolated LVNC patient

(A) Upper panel: pedigree I and II indicate generations. An asterisk indicates the proband. Open circles and open boxes indicate female and male normal individuals respectively. A closed circle indicates a phenotype-positive, genotype-positive individual. A hatched circle indicates a phenotype-positive, genotype unknown individual. The forward slash indicates deceased individuals. Lower panel: PCR-restriction fragment length polymorphism analysis. Digestion of the PCR products with Eco81I generates polymorphic restriction fragments of 201 bp (wild-type allele) and/or 185 bp (mutant allele). (B) DNA sequence analysis. A single nucleotide transition from thymine to guanine at nucleotide position 1678 of βMHC was identified. This mutation leads to a missense mutation of Met^{531} to an arginine residue. (C) Twelve-lead ECG of the proband (II-4). (D) A photograph of the heart of the proband (II-4) at autopsy. Features of the heart were consistent with isolated LVNC.

transgenic vector based on the mouse αMHC (the analogous gene of the human βMHC) clone 918 (Figure 2A). Nucleotides 1604 and 1614 of the coding region were mutated using site-directed mutagenesis. c.1604T>G resulted in a p.Met532Arg mutation, and c.1614C>G resulted in the deletion of the XhoI site without amino acid change and enabled us to distinguish the mutant cDNA from wild-type cDNA. PCR of gDNA revealed that we could obtain 17 transgenic lines (Figure 2B), and six independent lines expressing transgene-derived αMHC mRNA (Figure 2C). Densitometric analysis of PCR products revealed that each transgenic line had unique ratios of transgene (a 351 bp band) to endogenous (248 bp and 103 bp bands) αMHC, which could be used to distinguish each transgenic line. Among these transgenic lines, we chose line numbers 41 and 23 because they showed severe phenotypes and expressed more αMHC mRNA than the other transgenic lines.

The non-transgenic mice and transgenic mice seemed to grow normally. However, by 12 months of age 19% ($n=33$) and 20% ($n=20$) of mice died in transgenic mice lines 23 and 41 respectively, compared with only one death in 30 (3.3%) non-transgenic mice (Figure 3). Transgenic mice died sporadically without showing prominent organ diseases except cardiac hypertrophy. The most likely cause of death was sudden cardiac arrest.

Echocardiography

Echocardiography was performed in seven transgenic mice of line 41 and six non-transgenic littermates. All mice were 8–10 months old and the mean age was not significantly different between the groups. Representative echocardiograms are shown in Figure 4. The difference in mean values of LVEDD, LVESD and FS were not statistically significant between non-transgenic and transgenic mice of line 41 (Table 2). However, IVST and PWT were significantly greater in transgenic mice of line 41 compared with non-transgenic mice.

Myocardial histopathology and morphology showed that transgenic mice developed HCM and DCM

There were no significant differences between non-transgenic mice and transgenic mice at 1 month of

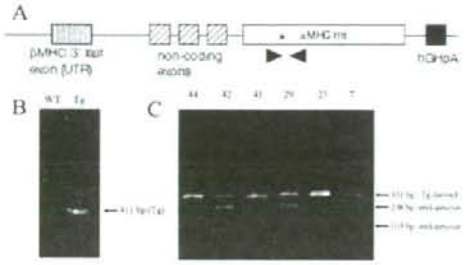

Figure 2 Transgenic construct and transcript expression

(A) A construct used to generate transgenic mice. Arrow heads indicate PCR primers for detection of αMHC cDNA. The asterisk indicates the position of the mutation (c.1604T>G). UTR, untranslated region; hGH pA, human growth hormone polyadenylation signal. (B) Identification of transgenic mice by PCR analysis of gDNA. A 411 bp PCR product was amplified using transgene specific primers for hGH pA. The 411 bp products are present only in the trangenic mice. (C) Analyses of transgene RNA expression by RT–PCR using primers in (A) in the hearts of six transgenic lines. When the PCR product (351 bp) was digested with XhoI, 248 bp and 103 bp fragments were generated from the endogenous allele, while the 351 bp fragment from the transgene was not digested, because the XhoI site was abolished by site-directed mutagenesis. Densitometric analysis of PCR products revealed that six transgenic lines (the number of the transgenic line is shown on each lane) had unique ratios of transgene to endogenous αMHC mRNA.

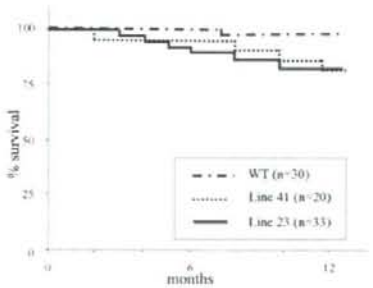

Figure 3 Survival curves of transgenic and non-transgenic mice

Non-transgenic mice (WT), $n = 30$; transgenic mice line 23, $n = 33$; transgenic mice line 41, $n = 20$.

age. Transgenic mice began to display left ventricular hypertrophy at 2–3 months of age, and showed left ventricular hypertrophy at about 12 months (Figure 5D). Striking histological and morphological abnormalities were observed in approx. 50% and 70% of transgenic mice of line 23 and line 41 respectively. When mice were approx. 18 months old, transgenic mice displayed enlarged atria and approx. 25% of transgenic mice progressed to exhibit left ventricular dilation compared with

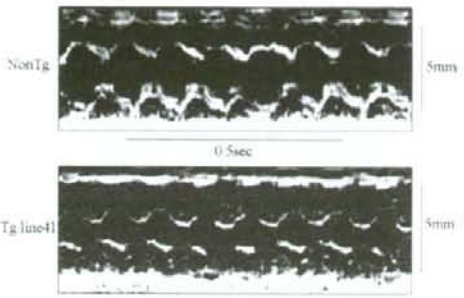

Figure 4 Echocardiographic analysis

Representative M-mode left ventricle images in 8- to 10 month old non-transgenic mice and transgenic mice line 41.

Table 2 Echocardiographic data in 8–10 month old non-transgenic mice and transgenic mice of line 41

Values are means ± S.D. HR, heart rate. $^*P < 0.05$ when compared with non-trangenic mice.

Parameter	Non-transgenic	Transgenic line 41
n	6	7
HR (beats/min)	590 ± 18	600 ± 13
LVEDD (mm)	3.57 ± 0.28	3.38 ± 0.30
LVESD (mm)	1.97 ± 0.18	1.84 ± 0.25
FS (%)	44.7 ± 2.0	45.7 ± 3.4
IVST (mm)	1.02 ± 0.08	1.16 ± 0.13*
PWT (mm)	1.01 ± 0.09	1.14 ± 0.11*

non-transgenic mice (Figures 5A–5C and 5E). However, transgenic mice did not show typical findings consistent with LVNC. Heart-to-body weight ratios at 12–15 months of age were significantly higher in transgenic mice compared with non-transgenic mice (Figure 6).

Histological examination of transgenic hearts revealed mild relative myocyte hypertrophy and myofibrillar disarray starting at 2–3 months of age. These features became more severe with aging. Multiple pleiotropic nuclei were also observed. These histological features were scattered throughout the left ventricular free wall. H and E- and Azan-stained sections of hearts from 15 month old mice showed interstitial fibrosis especially at the endocardium. Non-transgenic mice showed regular arrangement of myofibres and no fibrotic lesions (Figures 5F–5I).

Transmission electron microscopy was performed to examine the ultrastructure of transgenic and non-transgenic mice hearts at 16 months of age. The non-transgenic mice showed normal sarcomeric structure, with regularly aligned Z-bands (Figure 7A). In contrast, transgenic mice showed an abnormal sarcomeric structure. The sarcomere lengths were greatly reduced and the myofilaments were misaligned. The M-lines

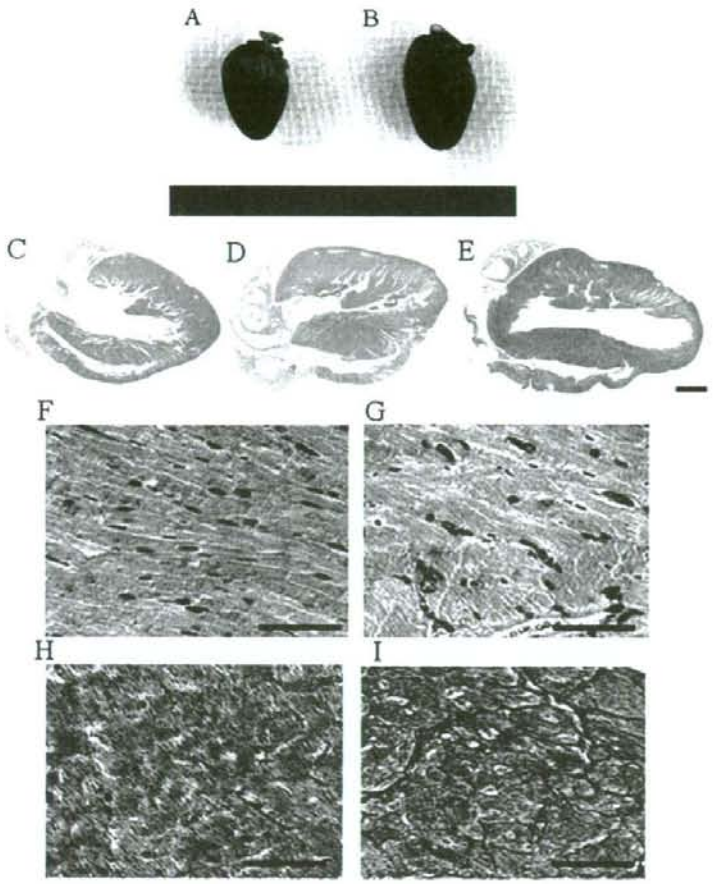

Figure 5 Histological analysis

Hearts were obtained from a non-transgenic mouse (A) and transgenic mouse line 41 (B) at 18 months of age. (C–E) Coronal sections of hearts stained with H and E. (C) Non-transgenic mouse (18 months old). (D) Transgenic mouse line 41 with left ventricular hypertrophy (12 months old). (E) Transgenic mouse line 41 with left ventricular dilation (18 months old). Scale bar represents 1 mm. Higher magnification views of H and E-stained left ventricle sections from a 15 month old non-transgenic (F) and transgenic mouse line 41 (G). Azan-stained sections of ventricles from a non-transgenic (H) and transgenic mouse line 41 (I). Scale bar represents 50 μm.

were indistinct and the Z-bands were thicker than those of non-transgenic mice (Figure 7B).

The expression level of βMHC (corresponding to αMHC in human), which is associated with a cardiac stress response, was compared in the hearts of transgenic mice of line 23 and transgenic mice of line 41 with non-transgenic mice at 4 months of age. Transgenic mice demonstrated significant increases in βMHC compared with age-matched non-transgenic mice (5.6-fold and 4.6-fold in lines 23 and 41 respectively). The amount of αMHC transcripts in transgenic hearts was the same as in age-matched non-transgenic hearts (Figure 8).

DISCUSSION

Generation of a novel transgenic mouse model having a point mutation in the αMHC gene that exhibits HCM developing to DCM

In the present study we have generated the first mouse model with a point mutation in the αMHC gene exhibiting HCM that developed to DCM, and it showed a more malignant phenotype compared with other αMHC mutant mice. At first, we identified a novel *de novo*

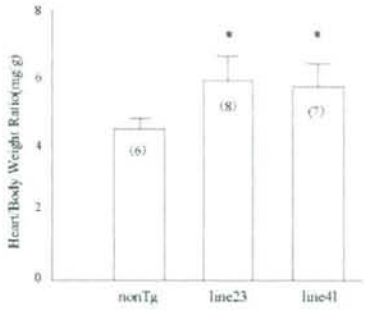

Figure 6 Ratios of heart-to-body weight for non-transgenic and transgenic mice of line 23 and line 41 at 12–15 months old

Bars represent means ± S.D. (n in parentheses). *$P < 0.05$ compared with non-transgenic mice.

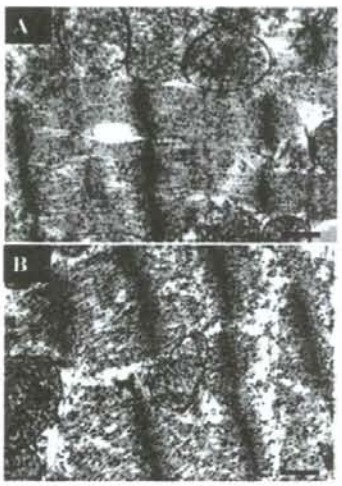

Figure 7 Electron micrographs of longitudinal sections of left ventricular cardiac myocyte cells from a non-transgenic mouse (A) and a transgenic mouse of line 23 (B) at 16 months

Scale bars represent 500 nm.

mutation in the βMHC gene in a patient with isolated LVNC, and generated αMHC transgenic mice with a p.Met532Arg missense mutation that is an analogous mutation of the patient. Although these mice did not develop LVNC, approx. 50–70% of them demonstrated the pathological and clinical features of human HCM after they were 2–3 months old. Moreover, 25% of transgenic mice progressed to exhibit DCM-like dilated phase HCM by 18 months of age. The phenotype of these p.Met532Arg αMHC transgenic mice is similar in

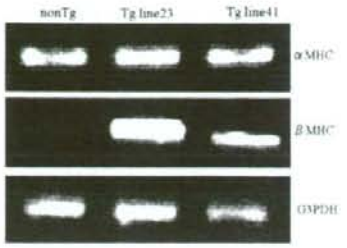

Figure 8 Semi-quantitative RT–PCR analysis of gene expression in hearts of 4-month-old mice

Expression levels of αMHC and βMHC were examined. The expression level of βMHC was increased 5.6-fold and 4.6-fold in transgenic mice line 23 and line 41 respectively. GAPDH was used as an internal control.

part to that of previously constructed αMHC transgenic mice models of HCM. It is not appropriate to compare the consequences of mutations by the severity of cardiac impairment of each mutant mouse because the amount of mutant cDNA expression and strains of mice are different. Nevertheless, our results suggest that the p.Met531Arg mutation may have more malignant consequences for cardiac function than other mutations in αMHC. For example, the mutation, p.Arg403Gln, in human βMHC caused severe HCM associated with early disease onset and short life expectancy in humans [23]. However, the p.Arg403Gln αMHC (analogous to human βMHC p.Arg403Gln) trangenic mice displayed mild cardiac dysfunction and hypertrophy with normal survival [24]. Compared with this p.Arg403Gln αMHC transgenic model, our p.Met531Arg αMHC transgenic mice progressed to severe left ventricular hypertrophy and further to dilated cardiomyopathy with sudden death. These results indicate that cardiac impairment of p.Met532Arg αMHC transgenic mice is significantly increased. In another model, αMHC transgenic mice bearing both the p.Arg403Gln mutation and a deletion in a part of the actin-binding site of αMHC evolved from left ventricular hypertrophy to dilation at 10 months of age even though only a small amount of transgenic protein was expressed (10% of endogenous αMHC protein) [10]. However, this model does not represent the real clinical consequence caused by p.Arg403Gln mutation in humans because the compound heterozygote of this mutation has not been identified to date in individuals with HCM. These results indicate that the phenotype of cardiomyopathy in mutant αMHC transgenic mice may be milder than that in humans.

Approx. 20% of our transgenic mice died by 12 months of age. The cause of death remains unknown because we could not evaluate the transgenic mice electrophysiologically due to technical difficulties. However, a previous study has reported that the degree of ventricular hypertrophy was significantly associated

with increased arrhythmia susceptibility in p.Arg403Gln αMHC transgenic mice [25]. Moreover, dead transgenic mice did not show the findings of heart failure or prominent diseases of other organs, except cardiac hypertrophy. These results suggest that these transgenic mice died of malignant arrhythmia. Further evaluation is necessary to clarify the electrophysiological abnormality in p.Met532Arg αMHC transgenic mice. *In vitro* functional studies may also help to elucidate the pathophysiological mechanisms affected by the p.Met531Arg mutation.

In the present study, p.Met532Arg αMHC trangenic mice did not show the phenotype of LVNC, unlike that found in the human patient. This result demonstrates that there is little impact of αMHC mutation on left ventricular morphogenesis. One explanation is that the expression pattern of αMHC in the murine heart is different from that of βMHC in the human heart. Human heart atria express αMHC and the ventricles express predominantly βMHC. In mouse, αMHC is expressed in both the postnatal atria and ventricles, whereas expression of βMHC in the embryonic ventricle is predominant over αMHC, especially when the process of ventricular myocardium compaction progresses. In mice, at 10.5 days post fertilization, αMHC gene expression begins to decrease in ventricular myocytes and trabeculations begin to form in the ventricles where βMHC is expressed dominantly [26]. Thus we speculate that the effect of βMHC mutation on left ventricle morphogenesis in humans may be much bigger than that of αMHC mutation in mice.

It is of note that the patient's monozygotic twin sister developed DCM. If the Met^{531} of βMHC was mutated to an arginine residue at the 1-cell stage, the twin sister had the same mutation. Although we could not examine this twin sister genetically because she died before the present study, it is possible that the p.Met531Arg mutation in βMHC caused DCM in her heart. Hence the transgenic model might reflect the pathology of human DCM rather than LVNC.

The mechanisms of onset of HCM and DCM

Met^{531} of βMHC is located in the actin-binding site. Replacement of a methionine residue by an arginine residue may impair the α-helix structure and disrupt the interaction between myosin and actin because methionine is a hydrophobic amino acid, whereas arginine is a basic and hydrophilic amino acid. Interestingly, other human DCM-causing mutations of βMHC are located near this region, such as p.Ser532Pro and p.Ala550Val [6,27]. For example, the p.Ser532Pro mutation which changes the charge of the amino acid at this position caused severe DCM. These results suggest that the p.Met531Arg mutation may cause catastrophic cardiomyopathy by a similar mechanism. Mutations in the genes encoding sarcomere proteins may alter contraction of cardiac muscle cells and activate multiple cellular pathways. When sarcomere proteins cannot interact sufficiently with other proteins because of the presence of mutations, cardiac remodelling may develop in order to compensate for the dysfunction, resulting in cardiomyopathy. It remains unclear why mutations of proteins with similar functions can cause two different morphologies, HCM and DCM, and whether these diseases are part of the same progressive pathology.

The results of the present study support the hypothesis that HCM and DCM reflect stages of a single progression pathway of heart disease [2]. Several studies of other mutant mice also support this hypothesis. For example, heterozygous mutant mice for the R403Q mutation developed HCM [25], whereas homozygous mutant mice developed DCM [11,12]. Furthermore, the R403Q mutation combined with a deletion in a part of the actin-binding site caused progression from HCM to DCM [26]. The fact that myohypertrophy is seen in DCM, and that HCM deteriorates into a phase that resembles DCM in human patients also supports the idea of a single pathophysiological progressive pathway.

In conclusion, the p.Met532Arg αMHC transgenic mice demonstrated a severe HCM phenotype with sudden death although they did not recapitulate the LVNC phenotype. In addition, some of the mice progressed to left ventricular dilation. These results indicate that the βMHC p.Met531Arg mutation contributes to malignant cardiomyopathy. This model would help to understand the pathological processes and aetiology of cardiomyopathy caused by MHC mutations.

ACKNOWLEDGMENTS

We thank T. Taniguchi and Y. Kubo (Kanazawa University Graduate School of Medicine, Kanazawa, Ishikawa, Japan) for excellent technical assistance.

REFERENCES

1 Richard, P., Charron, P., Carrier, L. et al. (2003) Hypertrophic cardiomyopathy: distribution of disease genes, spectrum of mutations, and implications for a molecular diagnosis strategy. Circulation **107**, 2227–2232
2 Seidman, J. G. and Seidman, C. (2001) The genetic basis for cardiomyopathy: from mutation identification to mechanistic paradigms. Cell **104**, 557–567
3 Marian, A. J. and Roberts, R. (1998) Molecular genetic basis of hypertrophic cardiomyopathy: genetic markers for sudden cardiac death. J. Cardiovasc. Electrophysiol. **9**, 88–99
4 Ahmad, F., Seidman, J. G. and Seidman, C. E. (2005) The genetic basis for cardiac remodeling. Annu. Rev. Genomics Hum. Genet. **6**, 185–216
5 Daehmlow, S., Erdmann, J., Knueppel, T. et al. (2002) Novel mutations in sarcomeric protein genes in dilated cardiomyopathy. Biochem. Biophys. Res. Commun. **298**, 116–120
6 Kamisago, M., Sharma, S. D., DePalma, S. R. et al. (2000) Mutations in sarcomere protein genes as a cause of dilated cardiomyopathy. N. Engl. J. Med. **343**, 1688–1696

7 Hecht, G. M., Klues, H. G., Roberts, W. C. and Maron, B. J. (1993) Coexistence of sudden cardiac death and end-stage heart failure in familial hypertrophic cardiomyopathy. J. Am. Coll. Cardiol. **22**, 489–497
8 ten Cate, F. J. and Roelandt, J. (1979) Progression to left ventricular dilatation in patients with hypertrophic obstructive cardiomyopathy. Am. Heart J. **97**, 762–765
9 Spirito, P. and Bellone, P. (1994) Natural history of hypertrophic cardiomyopathy. Br. Heart J. **72**, S10–S12
10 Vikstrom, K. L., Factor, S. M. and Leinwand, L. A. (1996) Mice expressing mutant myosin heavy chains are a model for familial hypertrophic cardiomyopathy. Mol. Med. **2**, 556–567
11 Fatkin, D., Christe, M. E., Aristizabal, O. et al. (1999) Neonatal cardiomyopathy in mice homozygous for the Arg403Gln mutation in the α-cardiac myosin heavy chain gene. J. Clin. Invest. **103**, 147–153
12 McConnell, B. K., Jones, K. A., Fatkin, D. et al. (1999) Dilated cardiomyopathy in homozygous myosin-binding protein-C mutant mice. J. Clin. Invest. **104**, 1235–1244
13 Mestroni, L., Maisch, B., McKenna, W. J. et al. (1999) Guidelines for the study of familial dilated cardiomyopathies. Eur. Heart J. **20**, 93–102
14 Jenni, R., Oechslin, E., Schneider, J. et al. (2001) Echocardiographic and pathoanatomical characteristics of isolated left ventricular non-compaction: a step towards classification as a distinct cardiomyopathy. Heart **86**, 666–671
15 Haliassos, A., Chomel, J. C., Tesson, L. et al. (1989) Modification of enzymatically amplified DNA for the detection of point mutations. Nucleic Acids Res. **17**, 3606
16 Jaenicke, T., Diederich, K. W., Haas, W. et al. (1990) The complete sequence of the human β-myosin heavy chain gene and a comparative analysis of its product. Genomics **8**, 194–206
17 Orita, M., Suzuki, Y., Sekiya, T. and Hayashi, K. (1989) Rapid and sensitive detection of point mutations and DNA polymorphisms using the polymerase chain reaction. Genomics **5**, 874–879
18 Mohabeer, A. J., Hiti, A. L. and Martin, W. J. (1991) Non-radioactive single strand conformation polymorphism (SSCP) using the Pharmacia 'PhastSystem'. Nucleic Acids Res. **19**, 3154
19 Lin, Z., Ohshima, T., Gao, S. et al. (2000) Genetic variation and relationships at five STR loci in five distinct ethnic groups in China. Forensic Sci. Int. **112**, 179–189
20 Nagai, A., Yamada, S., Watanabe, Y., Bunai, Y. and Ohya, I. (1996) Analysis of the STR loci HUMF13A01, HUMFXIIIB, HUMLIPOL, HUMTH01, HUMTPOX and HUMVWFA31 in a Japanese population. Int. J. Legal Med. **109**, 34–36
21 Chomczynski, P. and Sacchi, N. (1987) Single-step method of RNA isolation by acid guanidinium thiocyanate-phenol-chloroform extraction. Anal. Biochem. **162**, 156–159
22 Masami, S., Hidekazu, I., Toshihiko, Y. et al. (2005) Gene mutations in adult Japanese patients with dilated cardiomyopathy. Circ. J. **69**, 150–153
23 Watkins, H., Rosenzweig, A., Hwang, D. S. et al. (1992) Characteristics and prognostic implications of myosin missense mutations in familial hypertrophic cardiomyopathy. N. Engl. J. Med. **326**, 1108–1114
24 McConnell, B. K., Fatlin, D., Semsarian, C. et al. (2001) Comparison of two murine models of familial hypertrophic cardiomyopathy. Circ. Res. **88**, 383–389
25 Wolf, C. M., Moskowitz, I. P., Arno, S. et al. (2005) Somatic events modify hypertrophic cardiomyopathy pathology and link hypertrophy to arrhythmia. Proc. Natl. Acad. Sci. U.S.A. **102**, 18123–18128
26 Lyons, G. E., Schiaffino, S., Sassoon, D., Barton, P. and Buckingham, M. (1990) Developmental regulation of myosin gene expression in mouse cardiac muscle. J. Cell. Biol. **111**, 2427–2436
27 Villard, E., Duboscq-Bidot, L., Charron, P. et al. (2005) Mutation screening in dilated cardiomyopathy: prominent role of the β-myosin heavy chain gene. Eur. Heart J. **26**, 794–803

Received 31 May 2007/19 September 2007; accepted 23 October 2007
Published as Immediate Publication 23 October 2007, doi:10.1042/CS20070179

Mast Cells Play a Critical Role in the Pathogenesis of Viral Myocarditis

Hirokazu Higuchi, MD; Masatake Hara, MD, PhD; Kanjo Yamamoto, MD, PhD; Tadashi Miyamoto, MD, PhD; Makoto Kinoshita, MD, PhD; Tasuku Yamada, MD; Koji Uchiyama, MD; Akira Matsumori, MD, PhD

Background—Mast cells are powerful producers of multiple cytokines and chemical mediators playing a pivotal role in the pathogenesis of various cardiovascular diseases. We examined the role of mast cells in murine models of heart failure due to viral myocarditis, using 2 strains of mast cell–deficient mice.

Methods and Results—Two strains of mast cell–deficient mice, WBB6F1-Kit^{W}/Kit^{W-v} (W/W^{V}) and WCB6F1-$Kitl^{Sl}$/$Kitl^{Sl-d}$ (Sl/Sl^{d}), were inoculated with 10 plaque-forming units of the encephalomyocarditis virus intraperitoneally. On day 14 after inoculation, survival of W/W^{V} mice was significantly higher than that of their control littermates (77% versus 31%; $P=0.03$; n=13). On histological examination on day 7, myocardial necrosis and cellular infiltration were significantly less pronounced in W/W^{V} and Sl/Sl^{d} mice than in their control littermates (area of infiltration, 7.6±3.5% versus 29.3±15.6%; $P=0.002$; area of necrosis, 7.6±3.5% versus 30.0±17.2%; $P=0.003$; n=10). Histological examination showed more severe changes in mast cell–reconstituted than in –nonreconstituted W/W^{V} and Sl/Sl^{d} mice. The gene expressions of mast cell proteases were upregulated in the acute phase of viral myocarditis and rose further in the subacute phase of heart failure. Their activation coincided with the development of myocardial necrosis and fibrosis and correlated with the upregulation of gene expression of matrix metalloproteinase-9. The histamine H1-receptor antagonist bepotastine improved encephalomyocarditis viral myocarditis.

Conclusions—These observations suggest that mast cells participate in the acute inflammatory reaction and the onset of ventricular remodeling associated with acute viral myocarditis and that the inhibition of their function may be therapeutic in this disease. **(*Circulation*. 2008;118:363-372.)**

Key Words: cardiomyopathy ■ heart failure ■ immunology ■ inflammation ■ myocarditis ■ viruses

Viral myocarditis is an important cause of congestive heart failure (CHF) and dilated cardiomyopathy,[1] but its pathophysiology remains poorly understood. In recent years, mast cells have been implicated in the pathogenesis of cardiovascular and atherosclerotic disorders. In particular, we have observed that mast cells cause apoptosis of cardiac myocytes and proliferation of nonmyocytes in vitro.[2] Furthermore, myocardial histamine and tryptase content and mast cell density are higher in CHF due to idiopathic dilated or ischemic cardiomyopathy than in control hearts.[3] We showed that mast cells played a critical role in the progression of heart failure induced by pressure overload in mice.[4]

Clinical Perspective p 372

Mast cells are granulocytes known for their role in the pathogenesis of inflammatory diseases such as bronchial asthma, bacterial peritonitis,[5,6] rheumatic diseases,[7] and ulcerative colitis.[8] They produce several cytokines, including interleukin (IL)-1, IL-3, IL-4, IL-5, IL-6, interferon-γ, and tumor necrosis factor-α, mediators that are central in the development of inflammatory reactions.[9] Although they reside predominantly in tissues exposed to the outside environment, such as skin, intestinal tract, and trachea, mast cells are also normally present in the heart. They can be activated by several stimuli, including antibodies, cytokines, chemokines, and neuropeptides, eliciting a variety of responses, such as cell migration, the immediate release of inflammatory mediators, and selective cytokine production.[10–12] Because they are widely distributed in the form of premature precursors, these multifunctional cells are poised to play a pivotal role in the immune system. To mature, mast cell precursors require stimulation by stem cell factor (SCF) via c-kit, a transmem-

Received September 20, 2007; accepted May 23, 2008.

From the Department of Cardiovascular Medicine, Kyoto University Graduate School of Medicine, Kyoto (H.H., A.M.); Cardiovascular Division, Otsu Red-Cross Hospital, Shiga (H.H., M.H.); Cardiovascular Division, Wakayama Red-Cross Hospital, Wakayama (K.Y., T.Y.); Cardiovascular Division, Hyogo Prefectural Amagasaki Hospital, Hyogo (T.M.); Kobe City Medical Center General Hospital, Hyogo (M.K.); and Cardiovascular Division, Osaka Red-Cross Hospital, Osaka (K.U.), Japan.

A preliminary version of this manuscript was first received on December 18, 2004.

Correspondence to Akira Matsumori, MD, PhD, Department of Cardiovascular Medicine, Kyoto University, 54 Kawaracho Shogoin, Sakyo-ku, Kyoto 606-8397, Japan. E-mail amat@kuhp.kyoto-u.ac.jp

Circulation is available at http://circ.ahajournals.org DOI: 10.1161/CIRCULATIONAHA.107.741595

brane receptor with intrinsic tyrosine kinase activity.[11] The SCF–c-kit interaction stimulates them to migrate, proliferate, maturate, and survive.[13] SCF is expressed in a variety of tissue microenvironments, including the bone marrow, where mast cells normally begin their development. Therefore, the SCF–c-kit signal is key in the development of mast cell function.

The present study examined the role of mast cells in a mouse model of viral myocarditis using 2 strains of mast cell–deficient mice that have mutations in more upstream regulation, that is, SCF–c-kit mutations: (1) WBB6F1-Kit^{W}/Kit^{W-v} (W/W^{V}) mice, lacking the c-kit receptor, and (2) WCB6F1-Kitl^{Sl}/Kitl^{Sl-d} (Sl/Sl^{d}) mice, lacking SCF. Furthermore, we reconstituted mast cells by 2 methods in these mutant mice and studied the myocarditis tissues by microscopy and by quantitative reverse transcriptase polymerase chain reaction (PCR) analysis.

Methods

Animal Preparation

Genetically mast cell–deficient WBB6F1-Kit^{W}/Kit^{W-v} (W/W^{V}) mice, WCB6F1-Kitl^{Sl}/Kitl^{Sl-d} (Sl/Sl^{d}) mice, and their congenic littermates were purchased from the Jackson Laboratory (Bar Harbor, Me). Adult W/W^{V} mice and Sl/Sl^{d} mice ordinarily contain <1.0% of the number of dermal mast cells present in the skin of congenic littermates and have no detectable mature mast cells in the heart or other anatomic sites.[14,15]

Experimental Myocarditis Model

Stocks of the myocardiotrophic variant of encephalomyocarditis virus (EMCV) were prepared as described previously[1,16] and stored at −80°C. The 4-week-old male W/W^{V} (n=13 for survival experiments, n=10 for histopathological experiments) and Sl/Sl^{d} mice (n=10) used in this study were treated in accordance with local institutional guidelines at all stages of the experiments. They were inoculated with 0.2 mL EMCV intraperitoneally in phosphate-buffered saline diluted to a concentration of 50 plaque-forming units (pfu)/mL on day 0. The mice for survival experiments were observed daily for 14 days and were euthanized by cervical dislocation on day 7 for the histopathological experiments. The hearts were dissected, then 1 part was immediately frozen and stored at −80°C, and the other part was fixed in 10% formalin.

Mast Cell Reconstitution in Sl/Sl^{d} Mice by Repair of the Deficient Ligand SCF

Twelve 6-week-old WCB6F1-Sl/Sl^{d} mice were treated daily with subcutaneous recombinant murine SCF (rmSCF) (30 μg/kg per day in 0.2 mL of sterile 0.9% NaCl containing 0.1% bovine serum albumin fraction V, fatty acid free) for 21 days by the slightly modified method of Zsebo et al[17] and Tsai et al.[18] As a control group, 12 age-matched WCB6F1-Sl/Sl^{d} mice were treated subcutaneously with the vehicle alone, consisting of 0.1% bovine serum albumin in 0.9% NaCl. rmSCF was purchased from Pepro Tech EC Ltd (London, UK). Blood samples were obtained via the tail vein before and after treatment. Red and white blood cells, hemoglobin, and hematocrit in the peripheral blood were analyzed by Special Reference Laboratories (Tokyo, Japan). For the reconstituted mast cell analysis, heart, skin, and tongue tissues from 2 treated mice in each group were examined by toluidine blue staining. After confirmation of the mast cell reconstitution, 10 treated mice in each group were inoculated with 10 pfu of EMCV.

Mast Cell Reconstitution in W/W^{V} Mice by Transplantation of Bone Marrow–Derived Mast Cells

Mast cell deficiency was selectively and systematically treated in W/W^{V} mice by the injection of growth factor–dependent bone marrow–derived cultured mast cells (BMMC). Mast cells in 12 W/W^{V} mice were selectively reconstituted by the method of Nakano et al[15] and Martin et al[19] with a slight modification. Bone marrow cells were harvested from both femurs of 6-week-old wild-type female mice and cultured in complete RPMI 1640 media (Gibco BRL, Gaithersburg, Md) supplemented with 10% heat-inactivated FBS, 100 U/mL penicillin, 100 mg/mL streptomycin, and 2 mmol/L glutamine containing 50% WEHI-3 conditioned medium supernatant as an IL-3 source.[20] Half of the culture medium was replaced every 3 days. After 4 weeks of culture, cells were harvested and suspended in phosphate-buffered saline. Staining of the cells with Alcian blue solution confirmed that >95% of viable cells were mast cell progenitors. A total of 5×10^{6} BMMC^{c-kit+} in 0.2 mL of Eagle's medium were injected intravenously into twelve 6-week-old W/W^{V} mice. As a control group, 12 age-matched W/W^{V} mice received the Eagle's medium intravenously. Mast cell–reconstituted W/W^{V} mice were housed for 6 weeks; tissues from various organs were harvested from 2 treated mice in each group to confirm the reconstitution of mast cells. Inoculation with 10 pfu of EMCV was then performed in treated and control W/W^{V} mice.

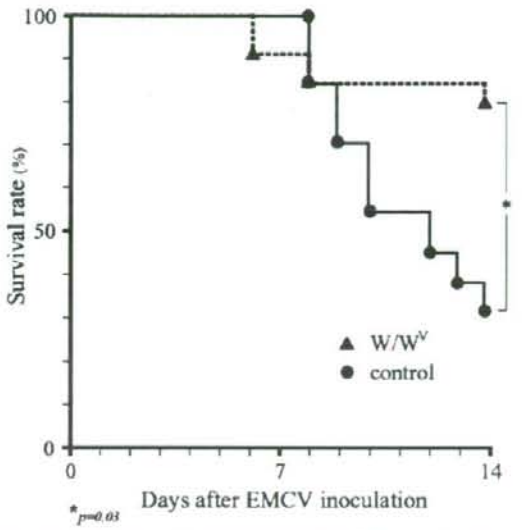

Figure 1. Kaplan–Meier survival curve in W/W^{V} mice. On day 14 after inoculation, the survival rate of W/W^{V} mice was significantly higher than that of their control littermates (77% vs 31%; P=0.03; n=13).

Histopathological Examination

The hearts from surviving mice were harvested on day 7, fixed in 10% formalin, and embedded in paraffin. The left ventricles were sliced perpendicular to the long axis and stained with hematoxylin-eosin and Masson trichrome for light microscopic examinations. The extent of inflammatory cell infiltration and myocardial necrosis was evaluated by measuring the ratio (%) of inflammatory cell infiltration or myocardial necrosis area to total left ventricle area on a microscopic slide, with the use of the Scion Image program.

Measurements of Viral Concentrations

Measurements of viral concentration in heart and brain harvested on day 7 were made by plaque assay methods as described previously.[21] Each value represents the average of 2 experiments. Virus concentrations are expressed as log (pfu/g tissue).

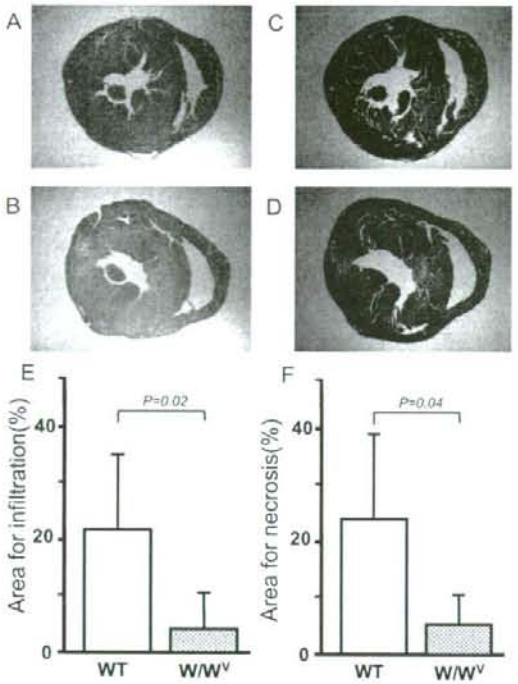

Figure 2. Histological examination of EMCV myocarditis in W/W^v mice. A and B, Hematoxylin-eosin stain. C and D, Masson trichrome stain. Inflammatory cell infiltration and myocardial necrosis in W/W^v mice (A and C) were less pronounced than in control littermates (B and D). E and F, Areas of inflammatory cell infiltration and myocardial necrosis were significantly less pronounced in W/W^v mice than in control littermates (4.3±5.0% vs 21.2±12.1%; P=0.02; 4.8±6.1% vs 23.9±16.6%, respectively; P=0.04). Values represent mean±SEM; n=10 in each group. WT indicates wild-type.

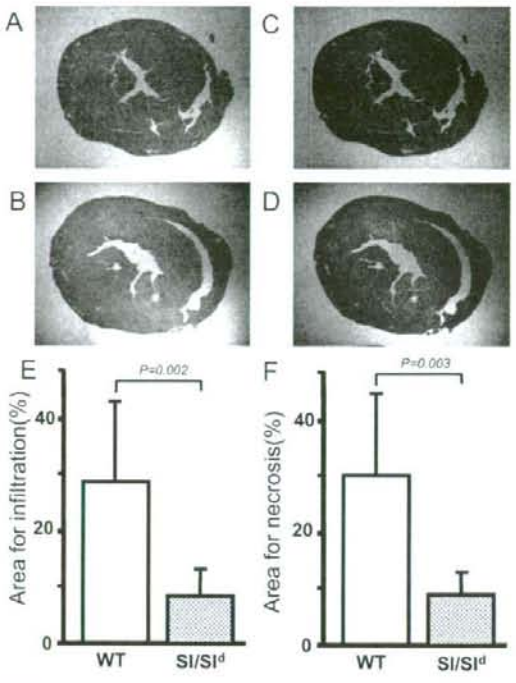

Figure 3. Histological examination in SI/SI^d mice. A and B, Hematoxylin-eosin stain. C and D, Masson trichrome stain. Inflammatory cell infiltration and myocardial necrosis in SI/SI^d mice (A and C) were less pronounced than in control littermates (B and D). E and F, Areas of inflammatory cell infiltration and myocardial necrosis were significantly less pronounced in SI/SI^d mice than in control littermates (7.6±3.5% vs 29.3±15.6%; P=0.002; 7.6±3.5% vs 30.0±17.2%, respectively; P=0.003). n=10 in each group. WT indicates wild-type.

Quantitative Reverse Transcriptase Polymerase Chain Reaction Analysis

Total RNA was isolated from the left ventricles by the acid guanidinium thiocyanate-phenol-chloroform method, and the RNA concentration was measured spectrophotochemically. First-strand cDNA was synthesized with the use of the SUPERSCRIPT Preamplification System for FirstStrand cDNA Synthesis (Gibco BRL). Real-time quantitative PCR (TaqMan PCR) with an ABI Prism 7700 Sequence Detection System and TaqMan PCR Core Reagent Kit (Perkin-Elmer Corp, Foster City, Calif) was performed according to the manufacturer's protocol. We used 2 mL of the first-strand cDNA in the following assay. The following forward (F) and reverse (R) oligonucleotides and probes (P) were used for the quantification of mouse mast cell protease (mMCP)-4, mMCP-5, matrix metalloproteinase-9 (MMP-9), IL-6, and glyceraldehydes-3-phosphate dehydrogenase mRNA: mMCP-4 F, 5'-GAAGTGAAAAGCCTGACCTGC-3'; mMCP-4 R, 5'-CATGCTTTGTTGAACCCA AGG-3'; mMCP-4 P, 5'-TGCATCAGAGTCTTCAAGCCAGAGCTC-3'; mMCP-5 F, 5'-TTGCCAGC CTGTGAGGAA A-3'; mMCP-5 R, 5'-TACAGACAGGCCAGATCGCAT-3'; mMCP-5 P, 5'-CTGGA ACTGGAATAGTGCAGGTTTTGTGTG-3'; MMP-9 F, 5'-TTGTGGTCTTCCCCAAAGACC-3'; MMP-9 R, 5'-TATCCACCGAGCCATCTGTCTA-3'; MMP-9 P, 5'-AAAACCTCCAACCTCACGGA CACCCA-3'; IL-6 F, 5'-CAGAATTGCCATCGTACAACTCTTTTCTCA-3'; IL-6 R, 5'-AAGTGCATC ATCGTTGTTCATACA-3'; IL-6 P, 5'-GAGGATACCACTCCCAACAGACC-3'; GAPDH F, 5'-TTCACCACCATGGAGAAGGC-3'; GAPDH R, 5'-GGCATGGACTGTGGTCATGA-3'; GAPDH P, 5'-TGCATCCTGCACCACCAACTGCTTAG-3'.

The conditions for the TaqMan PCR were as follows: 95°C for 10 minutes, followed by 40 cycles at 95°C for 15 seconds and 60°C for 1 minute.

Measurement of Active MMP-9 Activity in the Reconstituted W/W^v Mice Experiment

We measured active MMP-9 of the reconstituted W/W^v mice model using the Biotrak MMP-9 Activity Assay System from Amersham Biosciences (Piscataway, NJ). This assay is based on a 2-site enzyme-linked immunosorbent assay sandwich. Standards and samples are incubated in microtiter wells precoated with anti-MMP-9 antibody. Any MMP-9 present will be bound to the wells, whereas other components of the sample are removed by washing and aspiration. The total levels of free MMP-9 in a sample can be detected. To measure the total MMP-9 content, any bound MMP-9 in its pro form is activated with the use of *p*-aminophenylmercuric acetate. The standard is pro MMP-9, which is activated in parallel for both sample types. Active MMP-9 is detected through activation of the modified pro detection enzyme and the subsequent cleavage of its chromogenic peptide substrate. The resultant color is read at 405 nm in a microtiter plate spectrophotometer. The concentration of active MMP-9 in a sample is determined by interpolation from a standard curve.

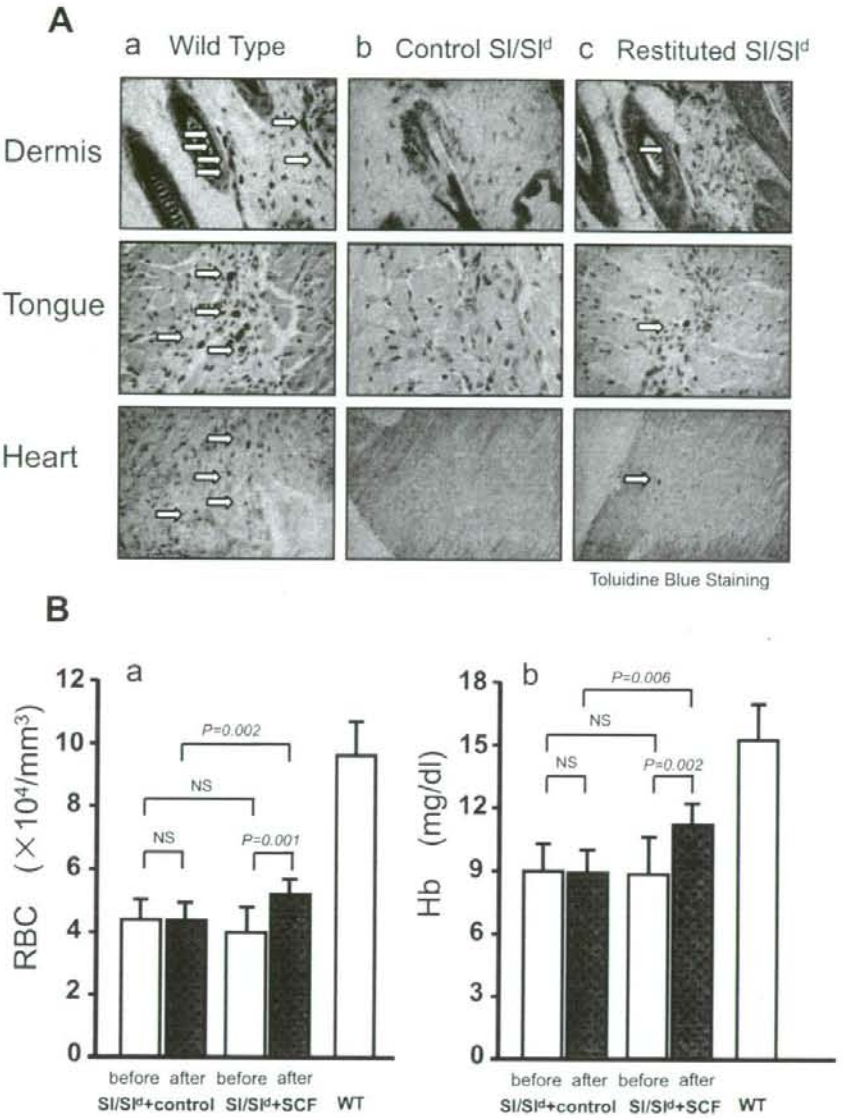

Figure 4. A, Mast cells in Sl/Sl^d mice reconstituted by rmSCF. Mast cells in dermis, tongue, and heart were detected by the metachromasia-positive granules (arrows). In control Sl/Sl^d mice (b), mast cells are absent. In Sl/Sl^d mice treated with rmSCF (c), mast cells are present, although their density is lower than in control littermates (a). B, Blood cell count in mast cell–reconstituted Sl/Sl^d mice. The red blood cell (RBC) count (a) and hemoglobin (Hb) (b) confirm a significant recovery from anemia with rmSCF. WT indicates wild-type.

Effect of Oral Histamine H1-Receptor Antagonist Bepotastine on EMCV Myocarditis in Mice

The histamine H1-receptor antagonist bepotastine besilate was obtained from Tanabe Seiyaku Co. Ltd. Osaka, Japan. The 4-week-old male DBA/2 mice were inoculated with EMCV as previously described. Bepotastine was dissolved in distilled water and given orally a dose of 10 mg/kg per day. Control mice were given distilled water. Survival (for 14 days, n=24 for each group) and histopathological changes on day 7 (n=12 for bepotastine group and n=8 for control) were examined as described previously.

Statistical Analysis

The survival rate of mice was analyzed by the Kaplan-Meier method, and survival differences between groups were tested by the log-rank test. Statistical comparisons of histological area and IL-6 were made by the unpaired 2-tailed Student t test. Comparisons of red blood cells and hemoglobin were made by the paired 2-tailed Student t test. Multiple comparisons among 3 groups were made by 1-way ANOVA and Newman-Keuls test for post hoc analysis. All values are presented as mean±SEM. Differences were considered statistically significant at probability values <0.05.

The authors had full access to and take full responsibility for the integrity of the data. All authors have read and agree to the manuscript as written.

Results

Murine Myocarditis in 2 Strains of Mast Cell–Deficient Mice

We inoculated W/W^v mice and Sl/Sl^d mice and their control littermates with 10 pfu of EMCV intraperitoneally. The survival rate of W/W^v mice on day 14 after inoculation (77%) was significantly higher than that of their control littermates (31%; P=0.03; n=13; Figure 1). On histological examination on day 7, myocardial necrosis and inflammatory cell infiltration were significantly less pronounced in both W/W^v (Figure 2A to 2F) and Sl/Sl^d mice (Figure 3A to 3F) than in their respective control littermates.

Reconstitution of Mast Cells in Sl/Sl^d Mice by Treatment With SCF

We reconstituted the mast cells in Sl/Sl^d mice by daily subcutaneous injections of rmSCF (30 μg/kg per day) for 21 days. At 4 weeks after the initial injection, we euthanized the mice and examined the distribution of mast cells in all tissues. We showed mast cells in skin, tongue, and myocardium (Figure 4A, a through c). Although the density of mast cells was low compared with that found in control littermates, we confirmed that they were distinctly reconstituted by the injections of rmSCF. Furthermore, examinations of the blood cell count showed a mean hemoglobin at 11.1±1.1 g/dL in Sl/Sl^d mice treated with rmSCF versus 9.2±1.5 g/dL in mice treated with the vehicle only (P=0.002; n=10 in each group; Figure 4B, b), consistent with a marked recovery from congenital macrocytic anemia from treatment with rmSCF.

We then inoculated both the treated Sl/Sl^d and the untreated Sl/Sl^d mice with 10 pfu of EMCV intraperitoneally. On day 7, myocardial necrosis and inflammatory cell infiltration were significantly more pronounced in reconstituted mast cells than in the untreated Sl/Sl^d mice (Figure 5A through 5F).

Transplantation of Bone Marrow–Derived Mast Cells to W/W^v Mice

We reconstituted the mast cells in W/W^v mice by transplanting bone marrow–derived mast cells (BMMC$^{c\text{-}kit^+}$). Bone marrow cells harvested from both femurs of 6-week-old male wild-type mice were left for 4 weeks in WEHI-3 medium to become mast cell progenitors. We verified by Alcian blue staining that >95% of cultured cells were mast cell progenitors (Figure 6A, a and b). No stem cell–like cells were detected in the preparation. Although mast cell progenitors contain acid polysaccharides that are dyed blue with Alcian blue, stem cell–like cells do not contain them. We could not confirm a significant change in the blood cell count before and after transplantation (hemoglobin before versus after transplantation, 12.8±0.7 versus 12.0±0.8 g/dL; P=NS; n=10 in each group). Mast cell progenitors were intravenously injected into 6-week-old W/W^v male mice, which were followed for 6 weeks. Microscopic confirmation of the whole body distribution of mast cells requires ≥26 weeks of observation.[18] However, in our model of EMCV myocarditis, mice aged >12 weeks do not reliably develop myocarditis. Therefore, after a shorter period (M1), we inoculated with 10 pfu of EMCV intraperitoneally the mast cell–reconstituted and the untreated W/W^v mice. On histological examination on day 7, myocardial necrosis and cellular infiltration were significantly more pronounced in the mast cell–reconstituted than in the untreated W/W^v mice (Figure 6B, a through f).

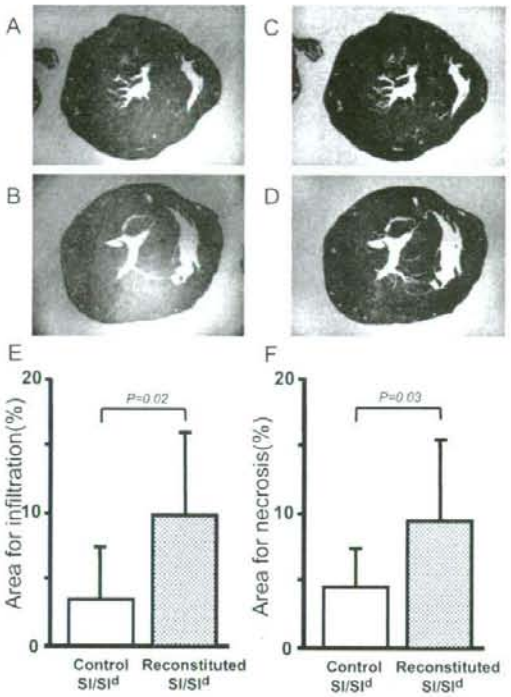

Figure 5. Histopathology in mast cell–reconstituted Sl/Sl^d mice. A and B, Hematoxylin-eosin stain. C and D, Masson trichrome stain. The histological changes of myocarditis were less marked than in 4-week-old mice in Figures 2 and 3 because the mice were 9 weeks old at the time of inoculation. The inflammatory cell infiltration and myocardial necrosis (E and F) were significantly more pronounced in reconstituted (B and D) than in control Sl/Sl^d (A and C) mice (9.4±6.9% vs 3.5±2.3%; P=0.02; 9.0±7.1% v;s 3.8±2.9%, respectively; P=0.03; n=10).

Measurements of Viral Concentrations

On day 7, no significant difference was found in the mean myocardial viral concentration between Sl/Sl^d mice and their control littermates (6.97±0.39 log [pfu]/g versus 7.17±0.43 log [pfu]/g; P=NS; n=10). Similar results were confirmed in the 2 reconstituted models (7.09±0.15 log [pfu]/g in Sl/Sl^d mice treated with rmSCF versus 6.99±0.24 log [pfu]/g in control mice; P=NS; n=10; 7.17±0.07 log [pfu]/g in mast cell–reconstituted W/W^v mice versus 7.18±0.04 log [pfu]/g in control W/W^v mice; P=NS; n=10). In addition, no significant difference was found in the mean brain viral concentration between W/W^v mice and control littermates (3.59±0.54 log [pfu]/g versus 2.94±0.56 log [pfu]/g; P=NS; n=5). Mast cells did not have an effect on intramyocardial viral concentrations.

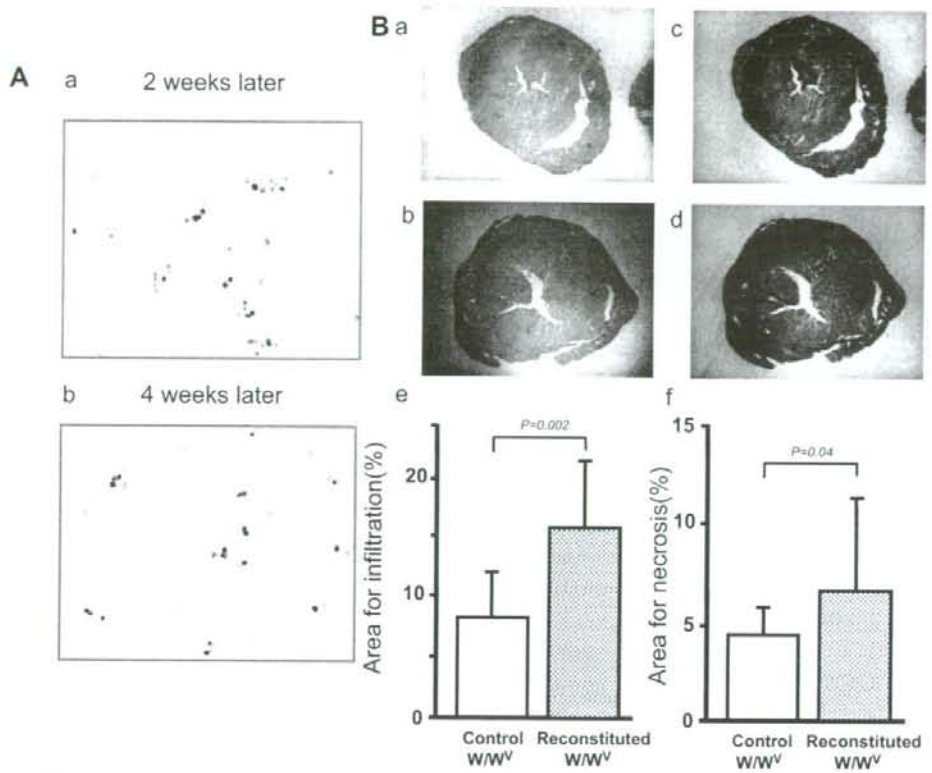

Figure 6. A, Culture of BMMC$^{c\text{-}kit+}$ stained with Alcian blue. The cells stained with Alcian blue are identified as premature BMMC$^{c\text{-}kit+}$. Two weeks later (a), the density of Alcian blue–positive cells was 50%. Four weeks later (b), it was near 95%. No stem cell–like cells were detected in the culture. B, Histopathology in mast cell–reconstituted W/W^{v} mice. a and b, Hematoxylin-eosin stain. c and d, Masson trichrome stain. The histological changes of myocarditis were less marked than in 4-week-old mice in Figures 2 and 3 because the mice were 12 weeks old at the time of inoculation. The inflammatory cell infiltration and myocardial necrosis (e and f) were significantly more pronounced in reconstituted (b and d) than in control W/W^{v} (a and c) mice (area of infiltration, 15.9±5.0% vs 8.2±4.9%; P=0.002; area of necrosis, 6.9±3.7% vs 4.1±1.6%; P=0.04; n=10).

Gene Expressions of Mouse Mast Cell Protease-4 and -5 and MMP-9 in the Heart of the Selective Mast Cell Reconstitution Model With Viral Myocarditis

No significant difference at baseline in gene expressions of mMCP-4 and -5 could be observed between uninfected and infected W/W^{v} mice (Figure 7A, a and b). In contrast, these gene expressions were significantly higher in the reconstituted than in the nonreconstituted W/W^{v} mice (Figure 7A, a and b). This confirmed that the mast cell reconstitution by BMMC$^{c\text{-}kit+}$ transplantation was successful and that the reconstituted mast cells participated prominently in the pathological process of viral myocarditis. Similar results were confirmed in the assessment of MMP-9 gene expression (Figure 7A, c) and in the measurements of active MMP-9 (Figure 7A, d). Finally, in this mast cell–reconstituted model, the gene expressions of mMCP-4 and -5 and MMP-9 were highly correlated (mMCP-4/MMP-9, r^2=0.9027, P<0.0001; mMCP-5/MMP-9, r^2=0.8665, P<0.0001; Figure 7B, a and b).

Cytokine Gene Expression in Myocardial Tissue

The gene expression of the proinflammatory cytokine IL-6 was significantly lower in Sl/Sl^{d} mice than in the control group (Figure 7C). In the model of mast cell reconstitution, it was significantly higher in mast cell–reconstituted W/W^{v} than in control W/W^{v} mice (Figure 7C).

Effect of Bepotastine on EMCV Myocarditis

Bepotastine improved survival and improved histopathological changes (Figure 8).

Discussion

In the study by El-Koraie et al,[22] mast cells and their associated growth factor (SCF) and receptor (c-kit) were present within the interstitium of scarred human kidneys and played a role in the initiation and progression of renal interstitial fibrosis. Frangogiannis et al[23] reported an increase in the number of mast cells in areas of collagen deposition and proliferating cell nuclear antigen expression and concluded that mast cells played an important role in myocardial remodeling and fibrosis after myocardial ischemia. Miyamoto

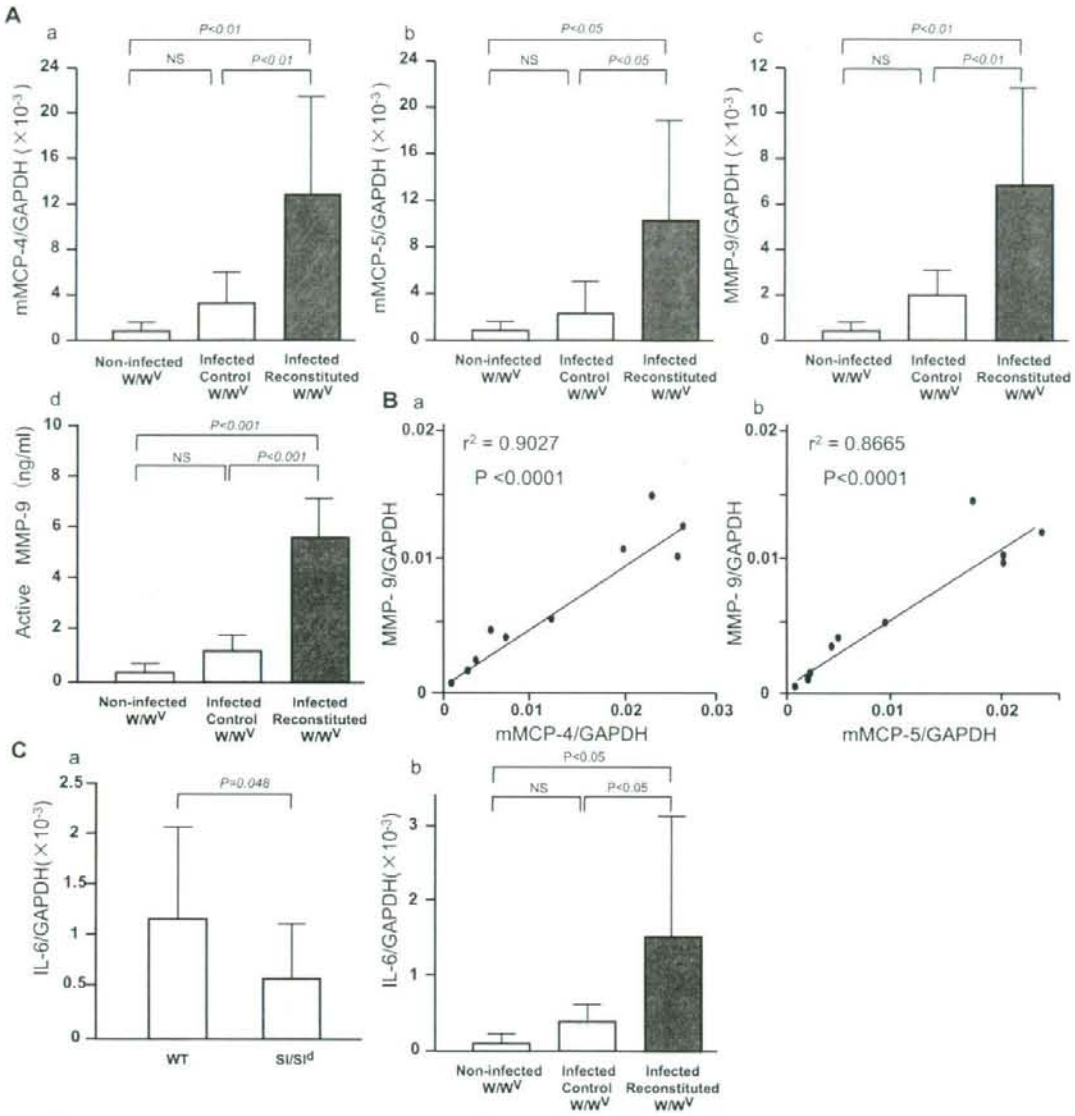

Figure 7. A, Reverse transcriptase PCR analysis in mast cell–reconstituted W/W^v mice. No significant difference was found in the gene expression of mMCP-4 and -5 between uninfected and infected W/W^v mice (mMCP4/GAPDH [10^{-3}], 0.5±0.2 vs 3.8±2.0; P=NS; mMCP-5/GAPDH [10^{-3}], 0.6±0.2 vs 3.3±2.0; P=NS) (a and b). The gene expressions of mMCP-4 and -5 were significantly greater in infected reconstituted than in infected nonreconstituted W/W^v mice (mMCP4/GAPDH [10^{-3}], 13.0±10.0 vs 3.8±2.0; P<0.01; mMCP-5/GAPDH [10^{-3}], 10.4±8.7 vs 3.3±2.0; P<0.05) (a and b). A similar result was observed in the gene expression of MMP-9 (noninfected W/W^v mice vs infected nonreconstituted W/W^v mice vs infected reconstituted W/W^v mice; MMP-9/GAPDH [10^{-3}], 0.065±0.26 vs 1.68±0.86 vs 6.64±5.01; P<0.05; n=10) (c) and its activity (activity of MMP-9 [ng/mL], 0.37±0.17 vs 1.51±0.33 vs 5.81±1.11; P<0.001; n=10) (d). B, Correlations between gene expression of mMCP-4 and -5 and MMP-9 in the reconstituted W/W^v mice. The gene expression of mMCP-4 and -5 and that of MMP-9 were highly correlated (mMCP-4/MMP-9, r^2=0.9027, P<0.0001; m-MCP-5/MMP-9, r^2=0.8665, P<0.0001) (a and b). C, Gene expression of the proinflammatory cytokine IL-6. It was significantly lower in mast cell–deficient mice (SI/SI^d) than in control mice (IL-6/GAPDH [×10^{-3}], 0.6±0.5 vs 1.2±0.9; P=0.048; n=10) (a). On the other hand, it was significantly higher in mast cell–reconstituted W/W^v mice than in control W/W^v mice (IL-6/GAPDH [×10^{-3}], 1.6±1.5 vs 0.5±0.2; P<0.05; n=10) (b).

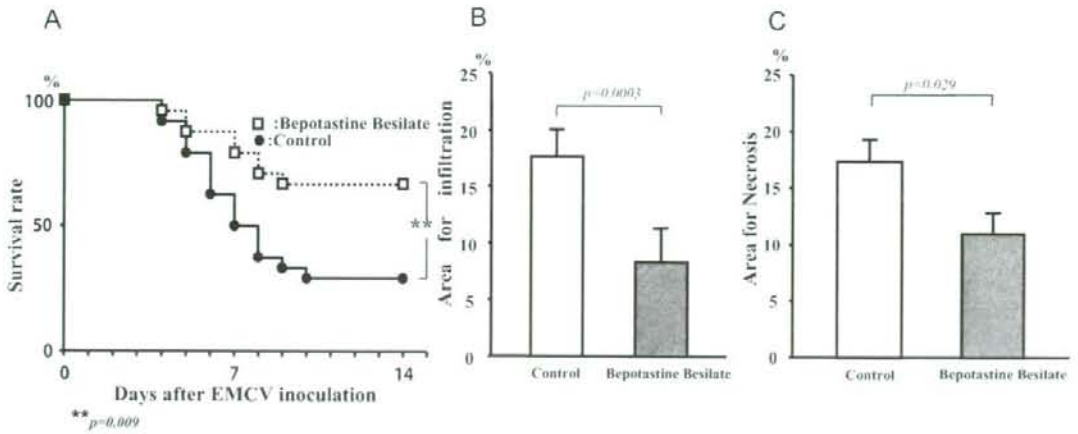

Figure 8. Effect of histamine H1-receptor antagonist bepotastine on EMCV myocarditis. Bepotastine significantly improved survival ($P=0.009$) (A) and decreased cellular infiltration (8.3 ± 3.1 vs 17.6 ± 3.0; $P=0.0003$) (B) and myocardial necrosis (17.1 ± 2.3 vs 11.0 ± 1.4; $P=0.029$) (C).

et al[24] observed that SCF mRNA was expressed in vitro and in vivo in human aortic endothelial and smooth muscle cells. This ability of endothelial and smooth muscle cells to interact with mast cells via SCF–c-kit receptor binding suggests that it plays a role in the metabolism of the arterial wall because SCF may be a most important factor influencing mast cell number, phenotype, and function in both health and disease. Kovanen et al[25] noted the local accumulation of mast cells in the highly vulnerable shoulder region of coronary atheromas and suggested that mast cell stimulation may trigger matrix degradation. Thus, mast cells are suspected to contribute to a late phase of acute inflammation.

We confirmed that the number of mast cells was increased on day 14 after EMCV inoculation, when myocardial fibrosis becomes apparent,[26] and that the protein level of SCF in the heart had already increased on day 7 in the EMCV myocarditis (H.H., MD, T.M., and A.M., unpublished data, 2002). Using our EMCV myocarditis model in these W/W^v and Sl/Sl^d strains of mice, we observed that mast cell deficiency had beneficial effects in this disorder. However, because these mutant mice suffer from macrocytic anemia, an important contributing factor in CHF, we reconstituted the mast cells by 2 methods to identify the independent role they may play.

In the reconstitution model by subcutaneous administration of rmSCF to Sl/Sl^d mice, both mast cell deficiency and macrocytic anemia were mitigated by active treatment because SCF was a ligand for c-kit. Although macrocytic anemia was mitigated by the reconstitution process, the histopathological severity of the lesions was greater in the reconstituted than in the nonreconstituted Sl/Sl^d mice. This observation strongly suggests the participation of mast cells in viral myocarditis. In the second mast cell reconstitution method by $BMMC^{c\text{-}kit+}$ transplantation from wild-type mice, the histopathological changes were, once again, more severe in the reconstituted than in the control W/W^v mice, further supporting the deleterious effects exerted by mast cells in viral myocarditis.

A multidisciplinary treatment to support the circulatory system in the acute stage of myocarditis is of critical importance, whereas, in the chronic stage, therapy should aim to prevent dilation of the cardiac chambers by limiting the development of cardiac fibrosis. MMPs, the endogenous system of extracellular matrix degradation and remodeling, are activated with the development of CHF.[27] In end-stage dilated cardiomyopathy, the ventricular content of MMP-3 and -9 increases, whereas that of MMP-2 remains unchanged compared with controls.[27] In cardiac remodeling, degradation and synthesis of the extracellular matrix occur simultaneously, resulting in ventricular chamber dilation. Mast cell chymase and tryptase, implicated in the degradation and synthesis of extracellular matrix, activate other MMPs including MMP-9.[28] Thus, the products of activated mast cells provide alternative MMP activation pathways.[29]

We have reported that the gene expression of mast cell chymase and tryptase was upregulated in the acute phase of viral myocarditis and rose further in the subacute phase of CHF.[26] This activation coincided with the development of myocardial necrosis and fibrosis and correlated with the upregulation of MMP-9 and type-I procollagen, suggesting that mast cell chymase and tryptase participate in the acute inflammatory reaction as well as the remodeling process associated with acute viral myocarditis.

The gene expression and activity of MMP-9[+] in mast cell–deficient mice was not significantly increased in the acute stage (day 7), although it was higher in mast cell–reconstituted W/W^v mice. This indicates that cardiac remodeling began in the acute stage of murine viral myocarditis and that mast cells and mast cell proteases may participate in the pathology of viral myocarditis.

Evidence is growing that proinflammatory cytokines play an important role in modulating cardiovascular function and structure.[30–32] Arteriovenous IL-6 spillover in the peripheral circulation increases with the severity of CHF, and an elevated level of plasma IL-6 was a predictor of mortality in

patients with CHF.[33] In the present study, the gene expression of IL-6 by the myocardial tissue was significantly increased in the mast cell–reconstituted W/W^{v} mice.

On the basis of our present results and numerous reports in the literature, we formed a hypothesis that mast cells are triggered in viral myocarditis to promote myocardial remodeling, contributing to the pathogenesis leading to CHF. Although mast cells are bone marrow–derived hematopoietic cells, committed mast cell progenitors circulate in small numbers in blood and are thought to migrate to the heart tissue before undergoing the final stage of maturation, including the development of mature granules. Mast cell progenitors can change their characteristics depending on their location and the surrounding environment, for example, depending on the site of inflammation. One of the most important features of mast cells is where they reside long term, that is, in close association with blood vessels at the site that is most likely to be exposed to pathogens.

Mast cells can detect and respond to pathogens depending on a combination of direct mechanisms including toll-like receptor–mediated activations and indirect mechanisms including Fc receptor–mediated or complement receptor–mediated activation.[34,35] In the heart tissue of our viral myocarditis model, activated mast cells release many proinflammatory cytokines such as IL-6 and tumor necrosis factor, mediators forming extracellular matrix such as MMPs, and fibrogenic mediators such as chymase and tryptase. Furthermore, these fibrogenic factors increase fibroblasts in the site of myocarditis and are supposed to produce SCF.[36,37] These SCF can mature and differentiate more mast cell precursors in the heart. Thus, mast cells play a critical role in the pathogenesis of viral myocarditis.

No treatment, aside from circulatory support, currently exists for severe acute viral myocarditis. The functions of mast cells can be controlled by antiallergic or antichemical mediator drugs. In fact, a histamine H1-receptor antagonist improved EMCV myocarditis. Our study therefore offers hope that the control of mast cells, for example, the interaction between SCF and c-kit, or the control of mast cell proteases may be effective in the management of viral myocarditis and subsequent CHF.

Acknowledgments

We would like to thank M. Ozone, M. Hayashi, and M. Shimada for preparing the manuscript.

Sources of Funding

This work was supported in part by a research grant from the Japanese Ministry of Health, Labor, and Welfare and a grant-in-aid for general scientific research from the Japanese Ministry of Education, Culture, Sports, Science, and Technology.

Disclosures

None.

References

1. Matsumori A, Kawai C. An experimental model for congestive heart failure after encephalomyocarditis virus myocarditis in mice. *Circulation*. 1982;65:1230–1235.
2. Hara M, Ono K, Hwang MW, Iwasaki A, Okada M, Nakatani K, Sasayama S, Matsumori A. Mast cells cause apoptosis of cardiomyocytes and proliferation of other intramyocardial cells in vitro. *Circulation*. 1999;100:1443–1449.
3. Patella V, Marino I, Arbustini E, Lamparter-Schummert B, Verga L, Adt M, Marone G. Stem cell factor in mast cells and increased mast cell density in idiopathic and ischemic cardiomyopathy. *Circulation*. 1998; 97:971–978.
4. Hara M, Ono K, Hwang MW, Iwasaki A, Okada M, Nakatani K, Sasayama S, Matsumori A. Evidence for a role of mast cells in the evolution to congestive heart failure. *J Exp Med*. 2002;195:375–381.
5. Huang C, Friend DS, Qiu WT, Wong GW, Morales G, Hunt J, Stevens RL. Induction of a selective and persistent extravasation of neutrophils into the peritoneal cavity by tryptase mouse mast cell protease 6. *J Immunol*. 1998;160:1910–1919.
6. Malaviya R, Ikeda T, Ross E, Abraham SN. Mast cell modulation of neutrophil influx and bacterial clearance at sites of infection through TNF-alpha. *Nature*. 1996;381:77–80.
7. Gotis-Graham I, Smith MD, Parker A, McNeil HP. Synovial mast cell responses during clinical improvement in early rheumatoid arthritis. *Ann Rheum Dis*. 1998;57:664–671.
8. King T, Biddle W, Bhatia P, Moore J, Miner PB Jr. Colonic mucosal mast cell distribution at line of demarcation of active ulcerative colitis. *Dig Dis Sci*. 1992;37:490–495.
9. Galli SJ, Wershil BK. Mouse mast cell cytokine production: role in cutaneous inflammatory and immunological responses. *Exp Dermatol*. 1995;4:240–249.
10. Galli SJ, Maurer M, Lantz CS. Mast cells as sentinels of innate immunity. *Curr Opin Immunol*. 1999;11:53–59.
11. Burd PR, Rogers HW, Gordon JR, Martin CA, Jayaraman S, Wilson SD, Dvorak AM, Galli SJ, Dorf ME. Interleukin 3-dependent and -independent mast cells stimulated with IgE and antigen express multiple cytokines. *J Exp Med*. 1989;170:245–257.
12. Gordon JR, Galli SJ. Mast cells as a source of both preformed and immunologically inducible TNF-alpha/cachectin. *Nature*. 1990;346: 274–276.
13. Galli SJ, Tsai M, Gordon JR, Geissler EN, Wershil BK. Analyzing mast cell development and function using mice carrying mutations at W/*c-kit* or Sl/MGF (SCF) loci. *Ann N Y Acad Sci*. 1992;664:69–88.
14. Kitamura Y, Go S, Hatanaka K. Decrease of mast cells in W/W^{v} mice and their increase by bone marrow transplantation. *Blood*. 1978;52:447–452.
15. Nakano T, Sonoda T, Hayashi C, Yamatodani A, Kanayama Y, Yamamura T, Asai H, Yonezawa T, Kitamura Y, Galli SJ. Fate of bone marrow-derived cultured mast cells after intracutaneous, intraperitoneal, and intravenous transfer into genetically mast cell-deficient W/W^{v} mice: evidence that cultured mast cells can give rise to both connective tissue type and mucosal mast cells. *J Exp Med*. 1985;162:1025–1043.
16. Kyu B, Matsumori A, Sato Y, Okada I, Chapman NM, Tracy S. Cardiac persistence of cardioviral RNA detected by polymerase chain reaction in a murine model of dilated cardiomyopathy. *Circulation*. 1992;86: 522–530.
17. Zsebo KM, Williams DA, Geissler EN, Broudy VC, Martin FH, Atkins HL, Hsu RY, Birkett NC, Okino KH, Murdock DC, Jacobsen FW, Langley KE, Smith KA, Takeishi T, Cattanach BM, Galli SJ, Suggs SV. Stem cell factor is encoded at the Sl locus of the mouse and is the ligand for the c-kit tyrosine kinase receptor. *Cell*. 1990;63:213–224.
18. Tsai M, Shih LS, Newlands GF, Takeishi T, Langley KE, Zsebo KM, Miller HR, Geissler EN, Galli SJ. The rat c-kit ligand, stem cell factor, induces the development of connective tissue-type and mucosal mast cells in vivo: analysis by anatomical distribution, histochemistry, and protease phenotype. *J Exp Med*. 1991;174:125–131.
19. Martin TR, Takeishi T, Katz HR, Austen KF, Drazen JM, Galli SJ. Mast cell activation enhances airway responsiveness to methacholine in the mouse. *J Clin Invest*. 1993;91:1176–1182.
20. Yung YP, Moore MA. Long-term in vitro culture of murine mast cells, III: discrimination of mast cells growth factor and granulocyte-CSF. *J Immunol*. 1982;129:1256–1261.
21. Matsumori A, Wang H, Abelmann WH, Crumpacker CS. Treatment of viral myocarditis with ribavirin in an animal preparation. *Circulation*. 1985;71:834–839.
22. El-Koraie AF, Baddour NM, Adam AG, El Kashef EH, El Nahas AM. Role of stem cell factor and mast cells in the progression of chronic glomerulonephritides. *Kidney Int*. 2001;60:167–172.
23. Frangogiannis NG, Perrard JL, Mendoza LH, Burns AR, Lindsey ML, Ballantyne CM, Michael LH, Smith CW, Entman ML. Stem cell factor induction is associated with mast cell accumulation after canine myocardial ischemia and reperfusion. *Circulation*. 1998;98:687–698.

24. Miyamoto T, Sasaguri Y, Sasaguri T, Azakami S, Yasukawa H, Kato S, Arima N, Sugama K, Morimatsu M. Expression of stem cell factor in human aortic endothelial and smooth muscle cells. *Atherosclerosis*. 1997;129:207–213.
25. Kovanen PT, Kaartinen M, Paavonen T. Infiltrates of activated mast cells at the site of coronary atheromatous erosion or rupture in myocardial infarction. *Circulation*. 1995;92:1084–1088.
26. Kitaura-Inenaga K, Hara M, Higuchi H, Yamamoto K, Yamaki A, Ono K, Nakano A, Kinoshita M, Sasayama S, Matsumori A. Gene expression of cardiac mast cell chymase and tryptase in a murine model of heart failure caused by viral myocarditis. *Circ J*. 2003;67:881–884.
27. Thomas CV, Coker ML, Zellner JL, Handy JR, Crumbley AJ III, Spinale FG. Increased matrix metalloproteinase activity and selective upregulation in LV myocardium from patients with end-stage dilated cardiomyopathy. *Circulation*. 1998;97:1708–1715.
28. Gruber BL, Marchese MJ, Suzuki K, Schwartz LB, Okada Y, Nagase H, Ramamurthy NS. Synovial procollagenase activation by human mast cell tryptase dependence upon matrix metalloproteinase 3 activation. *J Clin Invest*. 1989;84:1657–1662.
29. Fang KC, Raymond WW, Lazarus SC, Caughey GH. Dog mastocytoma cells secrete a 92-kD gelatinase activated extracellularly by mast cell chymase. *J Clin Invest*. 1996;97:1589–1596.
30. Matsumori A, Yamada T, Suzuki H, Matoba Y, Sasayama S. Increased circulating cytokines in patients with myocarditis and cardiomyopathy. *Br Heart J*. 1994;72:561–566.
31. Matsumori A. Cytokines in myocarditis and cardiomyopathies. *Curr Opin Cardiol*. 1996;11:302–309.
32. Matsumori A. Molecular and immune mechanisms in the pathogenesis of cardiomyopathy. *Jpn Circ J*. 1997;61:275–291.
33. Tsutamoto T, Hisanaga T, Wada A, Maeda K, Ohnishi M, Fukai D, Mabuchi N, Sawaki M, Kinoshita M. Interleukin-6 spillover in the peripheral circulation increases with the severity of heart failure, and the high plasma level of interleukin-6 is an important prognostic predictor in patients with congestive heart failure. *J Am Coll Cardiol*. 1998;31:391–398.
34. Heil F, Hemmi H, Hochrein H, Ampenberger F, Kirschning C, Akira S, Lipford G, Wagner H, Bauer S. Species-specific recognition of single-stranded RNA via toll-like receptor 7 and 8. *Science*. 2004;5:1526–1529.
35. Kulka M, Alexopoulou L, Flavell RA, Metcalfe DD. Activation of mast cells by double-stranded RNA: evidence for activation through toll-like receptor 3. *J Allergy Clin Immunol*. 2004;114:174–182.
36. Yamamoto T, Hartmann K, Eckes B, Krieg T. Role of stem cell factor and monocyte chemoattractant protein-1 in the interaction between fibroblasts and mast cells in fibrosis. *J Dermatol Sci*. 2001;26:106–111.
37. Fireman E, Kivity S, Shahar I, Reshef T, Mekori YA. Secretion of stem cell factor by alveolar fibroblasts in interstitial lung diseases. *Immunol Lett*. 1999;67:229–236.

CLINICAL PERSPECTIVE

Mast cells are multifunctional cells that contain various mediators such as cytokines, histamine, proteases, and leukotrienes. They are found in nearly all major organs of the body and are involved in many types of inflammation as well as allergic inflammation. Recently, we showed that the gene expressions of the mast cells chymase and tryptase were increased in the acute stages of heart failure and viral myocarditis, suggesting that viral infection may also activate mast cells. In the present study, survival of mice was better in mast cell–deficient mice infected with encephalomyocarditis virus and in association with less-pronounced myocardial necrosis, inflammation, and gene expressions of proinflammatory cytokines. Of note, all of these reactions were restored in mast cell–reconstituted mice. A histamine H1-receptor antagonist also alleviated viral myocarditis. These observations suggest that mast cells participate in the acute inflammatory reaction and the onset of ventricular remodeling associated with acute viral myocarditis and that the inhibition of their function may be therapeutic in this disease.

Human Molecular Genetics, 2008, Vol. 17, No. 4 **617–627**
doi:10.1093/hmg/ddm335
Advance Access published on November 14, 2007

High-density association study and nomination of susceptibility genes for hypertension in the Japanese National Project

Norihiro Kato[1,*], Toshiyuki Miyata[3], Yasuharu Tabara[4], Tomohiro Katsuya[6], Kazuyuki Yanai[1], Hironori Hanada[3], Kei Kamide[3], Jun Nakura[5], Katsuhiko Kohara[5], Fumihiko Takeuchi[2], Hiroyuki Mano[7], Michio Yasunami[8,9], Akinori Kimura[8,9], Yoshikuni Kita[10], Hirotsugu Ueshima[10], Tomohiro Nakayama[11], Masayoshi Soma[12], Akira Hata[13], Akihiro Fujioka[14], Yuhei Kawano[3], Kazuwa Nakao[15], Akihiro Sekine[16], Teruhiko Yoshida[17], Yusuke Nakamura[16,18], Takao Saruta[19], Toshio Ogihara[6], Sumio Sugano[20], Tetsuro Miki[5] and Hitonobu Tomoike[3]

[1]Department of Gene Diagnostics and Therapeutics and [2]Department of Medical Ecology and Informatics, Research Institute, International Medical Center of Japan, Tokyo, Japan, [3]National Cardiovascular Center, Suita, Osaka, Japan, [4]Department of Basic Medical Research and Education and [5]Department of Geriatric Medicine, Ehime University Graduate School of Medicine, Toon, Ehime, Japan, [6]Department of Geriatric Medicine, Osaka University Graduate School of Medicine, Suita, Osaka, Japan, [7]Division of Functional Genomics, Jichi Medical University, Shimotsuke-shi, Tochigi, Japan, [8]Department of Molecular Pathogenesis, Medical Research Institute and [9]Laboratory of Genome Diversity, School of Biomedical Science, Tokyo Medical and Dental University, Tokyo, Japan, [10]Department of Health Science, Shiga University of Medical Science, Otsu, Shiga, Japan, [11]Division of Molecular Diagnostics, Advanced Medical Research Center and [12]Division of Nephrology and Endocrinology, Department of Internal Medicine, Nihon University School of Medicine, Tokyo, Japan, [13]Department of Public Health, Graduate School of Medicine, Chiba University, Chiba, Japan, [14]Amagasaki Health Medical Foundation, Amagasaki, Hyogo, Japan, [15]Department of Medicine and Clinical Science, Kyoto University Graduate School of Medicine, Kyoto, Japan, [16]SNP Research Center, Institute of Physical and Chemical Research, Tokyo, Japan, [17]Genetics Division, National Cancer Center Research Institute, Tokyo, Japan, [18]Human Genome Center, Institute of Medical Science, University of Tokyo, Tokyo, Japan, [19]Department of Internal Medicine, School of Medicine, Keio University, Tokyo, Japan and [20]Division of Bioscience, Graduate School of Frontier Sciences, University of Tokyo, Tokyo, Japan

Received August 23, 2007; Revised and Accepted November 12, 2007

Essential hypertension is one of the most common, complex diseases, of which considerable efforts have been made to unravel the pathophysiological mechanisms. Over the last decade, multiple genome-wide linkage analyses have been conducted using 300–900 microsatellite markers but no single study has yielded definitive evidence for 'principal' hypertension susceptibility gene(s). Here, we performed a three-tiered, high-density association study of hypertension, which has been recently made possible. For tier 1, we genotyped 80 795 SNPs distributed throughout the genome in 188 male hypertensive subjects and two general population control groups (752 subjects per group). For tier 2 (752 hypertensive and 752 normotensive subjects), we genotyped a panel of 2676 SNPs selected (odds ratio $\geq$ 1.4 and $P \leq 0.015$ in tier 1) and identified 75 SNPs that showed similar tendency of association in tier 1 and tier 2 samples ($P \leq 0.05$ for allele frequency and $P \leq 0.01$ for genotype distribution tests). For tier 3 (619 hypertensive and 1406 normotensive subjects), we genotyped the 75 SNPs and found nine SNPs from seven genomic loci to be associated with hypertension

*To whom correspondence should be addressed at: Department of Gene Diagnostics and Therapeutics, Research Institute International Medical Center of Japan, 1-21-1 Toyama, Shinjuku-ku, Tokyo 162-8655, Japan. Tel: +81 332027181; Fax: +81 332027364; Email: nokato@ri.imcj.go.jp